

REPORT DOCUMENTATION PAGE

Form Approved
OMB No. 0704-0188

Public reporting burden for this collection of information is estimated to average 1 hour per response, including the time for reviewing instructions, searching existing data sources, gathering and maintaining the data needed, and completing and reviewing this collection of information. Send comments regarding this burden estimate or any other aspect of this collection of information, including suggestions for reducing this burden to Department of Defense, Washington Headquarters Services, Directorate for Information Operations and Reports (0704-0188), 1215 Jefferson Davis Highway, Suite 1204, Arlington, VA 22202-4302. Respondents should be aware that notwithstanding any other provision of law, no person shall be subject to any penalty for failing to comply with a collection of information if it does not display a currently valid OMB control number. PLEASE DO NOT RETURN YOUR FORM TO THE ABOVE ADDRESS.

1. REPORT DATE (DD-MM-YYYY)

28-05-2007

2. REPORT TYPE

Final Performance Report

3. DATES COVERED (From - To)

1 Nov. 2003 to 31 October 2006

4. TITLE AND SUBTITLE

Supercritical Fuel Pyrolysis

5a. CONTRACT NUMBER

5b. GRANT NUMBER

FA9550-04-1-0005

5c. PROGRAM ELEMENT NUMBER

61102F

6. AUTHOR(S)

Mary J. Wornat, Michelle L. Somers, Jennifer W. McClaine, Jorge O. Oña, and

Elmer B. Ledesma

5d. PROJECT NUMBER

2308

5e. TASK NUMBER

BX

5f. WORK UNIT NUMBER

7. PERFORMING ORGANIZATION NAME(S) AND ADDRESS(ES)

Louisiana State University
Department of Chemical Engineering
South Stadium Drive
Baton Rouge, LA 70803

8. PERFORMING ORGANIZATION REPORT NUMBER

9. SPONSORING / MONITORING AGENCY NAME(S) AND ADDRESS(ES)

AFOSR/NA
875 North Randolph Street
Suite 325, Room 3112
Arlington, VA 22203-1768

Dr Julian Tishkoff

10. SPONSOR/MONITOR'S ACRONYM(S)

11. SPONSOR/MONITOR'S REPORT NUMBER(S)

12. DISTRIBUTION / AVAILABILITY STATEMENT

Approved for public release; distribution is unlimited

AFRL-SR-AR-TR-07-0203

13. SUPPLEMENTARY NOTES

14. ABSTRACT

Supercritical pyrolysis experiments were conducted with three model fuels at temperatures up to 585 °C and pressures up to 110 atm. The products were analyzed by gas chromatography and high-pressure liquid chromatography with diode-array ultraviolet-visible absorbance and mass spectrometric detection, a technique ideally suited for the isomer-specific analysis of polycyclic aromatic hydrocarbons (PAH), which can serve as precursors to carbonaceous solids. Thirty-nine individual 2- to 9-ring PAH were identified in the supercritical 1-methylnaphthalene pyrolysis products—seventeen of which, for the first time. Reaction pathways involving 1-naphthylmethyl, methyl, and naphthyl radicals were developed to account for the formation of the observed PAH products and explain why unobserved PAH were not formed in the supercritical 1-methylnaphthalene pyrolysis environment. Likewise, reaction pathways involving benzyl, methyl, and phenyl radicals were developed that accounted for the formation of the forty-four individual PAH identified as supercritical toluene pyrolysis products and explained why unobserved PAH were not formed. The PAH product distribution from methylcyclohexane was extremely similar to that of toluene, indicating that the PAH formation mechanisms devised for toluene applied to supercritical methylcyclohexane as well.

15. SUBJECT TERMS

supercritical fuel pyrolysis, polycyclic aromatic hydrocarbons, carbonaceous solid deposits, hypersonic aircraft, PAH formation chemistry, high-pressure liquid chromatography, ultraviolet-visible absorption spectroscopy, mass spectrometry

16. SECURITY CLASSIFICATION OF:

a. REPORT
Unclassified

b. ABSTRACT
Unclassified

c. THIS PAGE
Unclassified

17. LIMITATION OF ABSTRACT

UL

18. NUMBER OF PAGES

76

19a. NAME OF RESPONSIBLE PERSON
Dr. Julian M. Tishkoff

19b. TELEPHONE NUMBER (include area code)
(703) 696-8478

Grant FA9550-04-1-0005: Supercritical Fuel Pyrolysis

Table of Contents

Cover Page	i
Table of Contents	ii
Background and Introduction	1
Experimental Equipment and Techniques	4
Reactor System	4
Product Analysis	5
Results and Discussion	8
Model Fuel Experiments with 1-Methylnaphthalene	9
Model Fuel Experiments with Toluene	27
Model Fuel Experiments with Methylcyclohexane	32
Analysis of Stressed Fischer-Tropsch Synthetic Jet Fuel S-8 from UTRC	33
Executive Summary	35
Summary of Results	35
Personnel who Performed the Research	38
Publications and Presentations	38
References	40
Tables	45
Figures	50

Background and Introduction

The fuels used in the next generation of hypersonic aircraft will have to operate under very high pressures and will have to sustain very high heat loads (*e.g.*, $\geq 30,000$ BTU/min) in order to meet aircraft cooling requirements [1-3]. Predictions indicate that within the fuel lines and injection system, where residence times can be several minutes, fuel temperatures and pressures may reach or exceed 540 °C and 150 atm [2]. These ranges of temperature and pressure substantially exceed the critical temperatures and pressures of most pure hydrocarbons and jet fuels such as JP-7 and JP-8 [1,4], so hydrocarbon fuels under these conditions will necessarily be supercritical fluids. These temperatures and pressures will also cause the fuel to undergo pyrolytic reactions, which have the potential of forming carbonaceous solids that can clog fuel lines, foul fuel nozzles, and lead to undesirable or even disastrous effects for the aircraft.

The current inability to predict solids formation tendencies of fuels under supercritical conditions has been brought to our attention by Dr. Tim Edwards (of the Air Force Research Laboratory, AFRL), who shared with us solid deposition results for various jet fuels and *n*-octane, from scramjet test rigs at United Technologies Research Center (UTRC) [5]. The tests show that the tendency to produce solid deposits increases in the order: JP-7 < RP-1 < JP-8+100 < JP-10 < *n*-octane—an order that would not have been predicted, based solely on the paraffins/naphthenes/aromatics contents in these fuels and the prevalent understanding of how these different component groups behave under pyrolysis conditions. Clearly we need to know more about the pyrolysis reactions of these fuels and fuel components under supercritical conditions. In order to develop reliable fuel systems for high-speed aircraft that will not be subject to solid deposit formation, we need a thorough understanding of the pyrolysis behavior of candidate fuels under the supercritical conditions that they will be operating. Of particular interest are the reactions leading to polycyclic aromatic hydrocarbons (PAH), which can serve as precursors to the carbonaceous solids.

The fact that the fuel pyrolysis environment is a supercritical one introduces several complexities. With regard to physical properties, supercritical fluids have highly variable

densities, no surface tension, and transport properties (*i.e.*, mass, energy, and momentum diffusivities) that are comparable to those of gases. Solvent-solute interactions, absent in the gas phase, can exhibit huge effects in supercritical fluids, often affecting chemical reaction pathways by facilitating the formation of certain transition states [6]. Because solvent-solute interactions are very dependent on pressure, chemical reaction rates in supercritical fluids can be highly pressure-dependent [6-9]. The kinetic reaction rate constant k has been shown [7,10] to vary exponentially with pressure, according to the expression $k = A_p \exp[(-\Delta V^\ddagger/RT)p]$, where A_p is the preexponential factor (in sec^{-1}) and ΔV^\ddagger is the activation volume (in L/mole). As the equation shows, a negative value of ΔV^\ddagger denotes that the reaction is favored by an increase in pressure. The magnitude of ΔV^\ddagger is an index of how sensitive the reaction rate is to pressure. For gases, ΔV^\ddagger is essentially zero; for liquids, ΔV^\ddagger is on the order of 10^{-2} L/mole; for supercritical fluids, ΔV^\ddagger is on the order of 1 to 10 L/mole [10].

For the case of fuel pyrolysis reactions, Stewart *et al.* [11,12] have demonstrated that reaction pathways and reaction kinetics indeed differ between the gas phase and the supercritical phase. Their pyrolysis experiments with decalin and methylcyclohexane in an atmospheric-pressure flow reactor and in the very supercritical pyrolysis reactor currently in our use show that under supercritical conditions—but not in the gas phase at atmospheric pressure—both decalin and methylcyclohexane are able to produce methylated C₅-ring intermediates that readily convert to structures containing 6-membered aromatic rings. These aromatic rings can then serve as kernels for further cyclic growth to PAH and ultimately carbonaceous solids. For the same two fuels, decalin and methylcyclohexane, Stewart *et al.* [11,12] also report different temperature-dependent global kinetic rate parameters A_T and E_a for their supercritical pyrolysis experiments, compared to their gas-phase experiments. Distinctions between the supercritical phase and gas phase are particularly pronounced for the reactions of PAH formation and growth. Studies in our laboratory with toluene demonstrate that acetylene-addition mechanisms [13-15]—widely applicable to high-temperature gas-phase combustion systems—do not hold for the lower temperatures and higher pressures of the supercritical fuel pyrolysis environment, as no acetylene is formed

[16,17]. We thus see that reaction pathways and reaction kinetics in the supercritical phase are substantially different from those in the gas or liquid phase. Therefore even for fuels whose gas-phase or liquid-phase pyrolysis behavior is well understood, it is of critical importance to study their pyrolysis in the supercritical phase, if these fuels are to be considered for future high-speed aircraft.

To that end, we have performed supercritical pyrolysis experiments with three model fuels: 1-methylnaphthalene, a two-ring aromatic component of jet fuels [18]; toluene, a one-ring aromatic component of jet fuels [18] and the major dehydrogenation product of the “endothermic” fuel methylcyclohexane; and methylcyclohexane itself. Because of the critical role that PAH play in the formation of carbonaceous solid deposits [16] and the need to discern PAH reaction pathways with as much specificity as possible, we have analyzed the products of the model fuel experiments by high-pressure liquid chromatography with diode-array ultraviolet-visible absorbance and mass spectrometric detection (HPLC/UV/MS), a technique ideally suited to the isomer-specific analysis of PAH. We have also employed HPLC/UV/MS in the compositional analysis of stressed Fischer-Tropsch synthetic jet fuel samples provided to us by Dr. He Huang of UTRC, at the instigation of Dr. Tim Edwards at AFRL.

In the following, we describe the supercritical fuels pyrolysis reactor used in the model fuel experiments and describe our product analysis procedures, explaining how the HPLC/UV/MS method works in the analysis of PAH. We then summarize the results we have obtained from the supercritical pyrolysis experiments with the three model fuels 1-methylnaphthalene, toluene, and methylcyclohexane—presenting the PAH formation reaction mechanisms that the experimental findings have helped us to devise for the fuels in the supercritical pyrolysis environment. The results of the HPLC/UV/MS analyses of one of the UTRC samples from a Fischer-Tropsch synthetic jet fuel are then presented, followed by a summary of all of the results presented in this report. Finally, we list the people who performed the research supported by Grant FA9550-04-1-0005 and the publications and conference presentations coming from that research.

Experimental Equipment and Techniques

Since most of the work performed for Grant FA9550-04-1-0005 involves the supercritical pyrolysis experiments with the model fuels, we first describe the reactor used in these experiments. We then describe the instruments and techniques used in the analyses of the products of these experiments as well as in the analyses of stressed fuel samples supplied to us by UTRC, at the instigation of Dr. Tim Edwards at AFRL.

Reactor System

The supercritical fuel pyrolysis experiments are conducted in the isothermal, isobaric reactor designed expressly for such purposes by Davis [19] and used by Stewart [11,12] in the AFOSR-sponsored research program supervised by Professor Irvin Glassman at Princeton University. Upon his retirement, Professor Glassman made the reactor available to us, and we have used it for supercritical fuel pyrolysis research over the last several years.

The reactor system [16,17,20] is illustrated in Figure 1. Prior to an experiment, liquid fuel is sparged with nitrogen for three hours [11] to remove any dissolved oxygen that could introduce auto-oxidative effects [21]. The sparged fuel is then loaded into a high-pressure pump, which delivers the fuel to the reactor, as shown in Figure 1. The reactor itself is a silica-lined stainless-steel coil of 1-mm i.d., 1.59-mm o.d. capillary tubing. (The silica lining prevents wall-catalyzed deposit formation that occurs with unlined stainless steel [11,19,21].) The reactor coil is immersed in a temperature-controlled fluidized-alumina bath, which ensures isothermality throughout the reactor length. As indicated in Figure 1, the entrance and exit lines of the reactor are passed through a water-cooled (25 °C) heat exchanger to ensure a controlled thermal history and residence time. Exiting the heat exchanger, the quenched reaction products pass through a stainless-steel filter (hole size, 10 μ m) and on to a high-pressure valve, for liquid product collection in the sample loop. Gaseous products are collected in a Teflon sampling bag following the high-pressure valve. A dome-loaded back-pressure regulator, downstream of the valve, controls the system pressure, to within ± 0.2 atm, up to a maximum of 115 atm.

Reactor residence time is varied by changing the length of the reactor coil or the flowrate. The reactor system is capable of operating at temperatures up to 585 °C, pressures up to 115 atm, and residence times up to several minutes. As documented by Davis [19] and Stewart [11], the reactor has been designed to meet Cutler's [22] and Lee's [23] criteria for idealization as plug flow, with regard to species concentration profiles. The resulting radially uniform species concentrations, coupled with the reactor's constant-temperature and constant-pressure operation, render this reactor ideal for supercritical pyrolysis kinetics experiments.

Product Analysis

At the conclusion of a pyrolysis experiment, the gaseous reaction products are removed and injected into an Agilent Model 6890N gas chromatograph (GC) with a flame-ionization detector (FID), for analysis of light-hydrocarbon gases. The liquid products are removed from the high-pressure collection valve and transferred to a vial. Most of the liquid product mixture is reserved for analysis by high-pressure liquid chromatography (HPLC), but a 20- μ L aliquot of the liquid product mixture is removed for injection onto an Agilent Model 6890 GC with a FID, in conjunction with an Agilent Model 5973 mass spectrometer (MS). The GC/FID/MS instrument is used to quantify the 1- to 2-ring (and sometimes 3- or 4-ring) liquid aromatic products—all of which are identified by matching retention times and mass spectra with those of reference standards.

The portion of the liquid product mixture reserved for HPLC analysis is concentrated in a Kuderna-Danish apparatus and exchanged, under nitrogen, into 200 μ L of dimethylsulfoxide, a solvent compatible with the solvents used in the HPLC methods [17,20] employed for PAH analysis. During the concentration and solvent-exchange procedure, portions of the more volatile aromatics, such as the 1- and 2-ring species, are lost to vaporization; hence these lighter aromatic products are quantified by gas chromatographic analysis, as described above.

For analysis of the large aromatic products (≥ 3 rings) by HPLC, two separate 20- μ L aliquots of the product/dimethylsulfoxide solution are injected onto two separate high-pressure liquid chromatographs—one, a Hewlett-Packard Model 1050, coupled to a diode-array ultraviolet-

visible (UV) absorbance detector; the other, an Agilent Model 1100, coupled to a diode-array UV detector in series with a mass spectrometer (MS). Each HPLC instrument uses a reversed-phase Restek Pinnacle II PAH octadecylsilica column (particle size, 5 μm ; inner diameter, 4.6 mm; and length, 250 mm). A time-programmed sequence of solvents—acetonitrile/water, acetonitrile, and dichloromethane—is pumped through the HPLC column, and the PAH product components elute in the order of increasing molecular size. An alternative solvent program—using methanol/water, methanol, and dichloromethane—is employed in some cases, to optimize separation of the large PAH. UV absorbance spectra are taken every 0.8 sec on the HPLC/UV (and every 0.4 sec on the HPLC/UV/MS) of the separated components as they exit the HPLC column. The diode-array UV detectors of both HPLC instruments monitor absorbance from 190 to 520 nm, the full range of UV wavelengths over which the product PAH absorb. Mass spectra are taken of the components after they leave the UV detector of the Agilent instrument. The MS employs atmospheric-pressure photo ionization and simultaneously monitors two ranges of mass-to-charge ratio: 75 to 500 and 273 to 550, with a cycle time of 1.02 sec.

The mass spectrum establishes the C_xH_y formula of the PAH, its molecular mass, and whether there are any substituent groups like methyl attached to the aromatic structure. The UV spectrum establishes the exact aromatic structure of the PAH, so for unsubstituted PAH, the UV spectrum alone is sufficient to establish the exact isomer-specific identity. If a PAH has an alkyl substituent, the UV spectrum looks almost exactly like that of the parent PAH, only shifted a few nm to higher wavelength—the position and length of the substituent dictating the details of the shift [24,25]. Therefore, for large PAH, which have a multitude of sites at which substituents can be located, one must have reference standards of all possible positional isomers in order to be certain of the exact position of the alkyl substituent—a condition rarely met. Consequently, for each of the alkylated PAH products of ≥ 5 rings reported in the Results and Discussion section of this Report, the exact structure of the aromatic portion of the PAH is known (from the UV spectrum); only the exact position of the alkyl group is uncertain.

PAH products from the supercritical fuel pyrolysis experiments are identified by matching HPLC retention times, mass spectra, and UV absorbance spectra with those of our PAH reference standards, which include both commercially available compounds as well as PAH that have been specially synthesized for our identification efforts. In some cases, in which reference standards are not available, product identities are established by matching UV spectra with those published in the literature for those compounds. Quantification of the identified PAH comes from extensive calibration of the HPLC instrument with reference standards, taking into account nonlinearities in the response of diode-array detectors at high analyte concentrations [26].

Since the number of possible PAH structures grows exponentially with ring number [25], the HPLC/UV/MS technique is particularly well suited for analyzing the large PAH molecules that are precursors to fuel-line carbonaceous solids. The HPLC separates each product component; the mass spectrum narrows the field of possible component identities to a particular C_xH_y isomer group; the fingerprint UV spectrum then permits the designation of the exact molecular structure of the product component.

The HPLC/UV/MS separation and identification method is illustrated in Figure 2, an HPLC chromatogram of a mixture of PAH reference standards. The peaks in the chromatogram represent individual components of the original mixture, which the HPLC has separated by the flow of solvents through the HPLC column. For any given component, such as the one eluting at 44.4 minutes in Figure 2, the HPLC/UV/MS instrument's computer records the component's mass spectrum and UV spectrum as the component is eluting from the HPLC column. The component eluting at 44.4 min in Figure 2, for example, has the mass spectrum that is the left inset of Figure 2 and the UV spectrum that is the right inset of Figure 2. For PAH subjected to atmospheric-pressure photo ionization in our HPLC/UV/MS system, the primary ion exhibited by the mass spectrum is dependent on the solvent running through the HPLC at the time the component is eluting. If the solvent is acetonitrile, such as is the case in Figure 2, the primary ion is at $m/z = M$, the molecular mass of the PAH. If the solvent is dichloromethane or methanol, such as is the case in some examples to be illustrated in the Results and Discussion, proton

transfer from the solvent [27] causes the primary ion in the PAH mass spectrum to be at $m/z = M+1$. In either case, the mass spectrum establishes the C_xH_y formula of the separated PAH component— $C_{22}H_{12}$ (from $M = 276$) for the component eluting at 44.4 min in Figure 2. The UV spectrum of this same component, shown as the black curve in the right inset of Figure 2, establishes exactly which $C_{22}H_{12}$ PAH this component is—benzo[ghi]perylene in this case, since the component's UV spectrum matches that of the reference standard of benzo[ghi]perylene, shown in red. The identity of the mixture component eluting at 44.4 min in Figure 2, is thus unequivocally established as benzo[ghi]perylene.

Since benzo[ghi]perylene is readily available as a reference standard from commercial sources, its identification would have been very straight forward simply from its UV absorbance spectrum, and the mass spectrum would not have been necessary. However, for larger-ring-number PAH, for which the number of possible isomers is huge (hundreds or even thousands) and reference standards are scarce, the mass spectrum provides information critically helpful to PAH identification, since it narrows the field of possible candidates down to a particular isomer family. Examples are demonstrated in the Results and Discussion section to follow.

Results and Discussion

Using the reactor of Figure 1, we have conducted supercritical pyrolysis experiments with three model fuels: 1-methylnaphthalene, a two-ring aromatic component of jet fuel [18]; toluene, a single-ring component of jet fuel [18] and the major dehydrogenation product of the endothermic fuel methylcyclohexane; and methylcyclohexane itself. The products of the experiments have been analyzed by HPLC/UV and/or HPLC/UV/MS, and the results are reported below, by fuel, in the order: 1-methylnaphthalene, toluene, methylcyclohexane. Following the results on the model fuels, results are presented on our compositional analyses of stressed Fischer-Tropsch synthetic jet fuel samples provided to us by Dr. He Huang at United Technologies Research Center, at the instigation of Dr. Tim Edwards at AFRL.

Model Fuel Experiments with 1-Methylnaphthalene

Supercritical pyrolysis experiments have been conducted in the reactor of Figure 1, with the model fuel 1-methylnaphthalene (critical temperature, 499 °C; critical pressure, 36 atm), a two-ring aromatic component of jet fuel [18] and one of the eleven constituents composing UTRC's simulated JP-8+100 fuel [28]. The experiments have been performed at temperatures of 550, 575, and 585 °C, at pressures of 40 to 110 atm, and at a fixed residence time of 140 sec. We focus here on the results of the experiments conducted at 585 °C and 110 atm, as this condition corresponds to the early stages of carbonaceous solids formation, at approximately 50% 1-methylnaphthalene conversion [20].

Figure 3 presents the HPLC chromatogram [20] of the aromatic products of 1-methylnaphthalene pyrolysis at 585 °C, 110 atm, and 140 sec. In addition to that of 1-methylnaphthalene itself (unreacted fuel), Figure 3 displays the structures of the 38 individual two- to seven-ring PAH products that have been identified by HPLC/UV/MS, as well as the molecular masses of the eight- and nine-ring PAH products whose exact identities are not yet known. (The clusters of peaks representing the > 30 bi-naphthyl products are also labelled in Figure 3.) Sixteen of the PAH of ≥ 5 rings in Figure 3 have never before been identified as products of 1-methylnaphthalene pyrolysis or combustion, so before discussing the mechanisms responsible for the formation of the products in Figure 3, we first present the HPLC, UV, and MS evidence [29] that establishes these products' identifications.

Identification of Products of Supercritical 1-Methylnaphthalene Pyrolysis

In order to facilitate discussion of the new product identifications, we present the same 1-methylnaphthalene products chromatogram of Figure 3 as Figure 4, but this time with each one of the newly identified product PAH labelled with either a single letter (for the unsubstituted PAH) or with a letter and a number (for the methylated PAH). These sixteen newly identified products

[29] include nine dibenzofluorenes—dibenzo[*a,i*]fluorene (**A**) and three of its methylated derivatives (**A1**, **A2**, and **A3**), dibenzo[*a,g*]fluorene (**B**) and one methylated dibenzo[*a,g*]fluorene (**B1**), and three methylated dibenzo[*a,h*]fluorenes (**C1**, **C2**, and **C3**)—as well as seven benzenoid PAH: benzo[*c*]chrysene (**D**), naphtho[2,1-*a*]pyrene (**E**) and three of its methylated derivatives (**E1**, **E2**, and **E3**), naphtho[2,3-*a*]pyrene (**F**), and dibenzo[*cd,lm*]perylene (**G**). The spectral evidence to support the 16 new product identifications is presented in the following. For unsubstituted PAH, only UV spectral matches are given since UV spectra provide sufficient unequivocal evidence for the identification of these products. For the methylated PAH, mass spectral evidence is also reported to establish the presence of the single methyl substituent. We first consider the nine newly identified dibenzofluorenes, then the seven newly identified benzenoid PAH.

Dibenzofluorenes. Among the products of 1-methylnaphthalene supercritical pyrolysis, two exhibit a molecular mass of 266 and seven exhibit a molecular mass of 280. A molecular mass of 266 corresponds to a PAH with formula $C_{21}H_{14}$; a molecular mass of 280, to its methyl-substituted counterpart, $CH_3-C_{21}H_{13}$. The following details the identifications of the nine $C_{21}H_{14}$ and $CH_3-C_{21}H_{13}$ dibenzofluorene products.

*Dibenzo[*a,i*]fluorenes.* Figure 5 displays the UV spectrum of the molecular mass (M) 266 1-methylnaphthalene pyrolysis product labelled **A**, eluting at 40 minutes in Figure 4. Also shown in Figure 5 is the UV spectrum of a reference standard of dibenzo[*a,i*]fluorene, obtained from the literature [30,31]. The UV spectral match confirms the identity of the M 266 product as the unsubstituted PAH dibenzo[*a,i*]fluorene.

Figure 6 displays the UV spectrum of the component labelled **A1** in Figure 4 and that of dibenzo[*a,i*]fluorene. The UV spectrum of component **A1** matches very closely with that of dibenzo[*a,i*]fluorene, only shifted ~3 nm to higher wavelength with reference to the UV spectrum of dibenzo[*a,i*]fluorene. The small (~2-3 nm) bathochromic shift in the UV spectrum indicates

[24,25] that component **A1** has the base structure of dibenzo[*a,i*]fluorene, along with a nonconjugating substituent group such as an alkyl functionality. The mass spectrum of component **A1**, in the inset of Figure 6, reveals that the primary ion is at $M = 280$, which corresponds to $\text{CH}_3\text{-C}_{21}\text{H}_{13}$, the molecular formula of a methyldibenzofluorene. The UV and mass spectra of component **A1** in Figure 6 thus establish the identity of component **A1** as a methyldibenzo[*a,i*]fluorene.

Two additional components in the chromatogram of Figure 4, labelled **A2** and **A3**, exhibit mass and UV spectra very similar to those of component **A1** in Figure 6, with only slight differences in the bathochromic shifts of the UV spectra. Components **A2** and **A3** are thus also methyldibenzo[*a,i*]fluorenes. The different HPLC elution times of the three product methyldibenzo[*a,i*]fluorenes—components **A1**, **A2**, and **A3**—indicate that the three isomers differ by the position of the methyl substituent. Without reference standards of all seven of the methyldibenzo[*a,i*]fluorenes, we cannot deduce, from our HPLC/UV/MS data alone, the positions of the methyl substituents in components **A1**, **A2**, and **A3**. The dominant presence of 1-methylnaphthalene in the reaction environment, however, and our findings concerning reaction pathways [20] strongly suggest that the 1, 4, and 5 positions are the most likely positions for the methyl groups in our three methyldibenzo[*a,i*]fluorene products. Figure 7 displays the structures of the 1-, 4-, and 5-methyldibenzo[*a,i*]fluorenes—the only three of the seven isomers of methyldibenzo[*a,i*]fluorene that fully preserve the intactness of the two 1-methylnaphthalene units involved in their construction.

It might be noted that, of the three isomers shown in Figure 7, 1-methyldibenzo[*a,i*]fluorene would be expected to elute earliest on the HPLC, due to the proximity of its methyl group to the two hydrogens of the methylene carbon. 1-methyldibenzo[*a,i*]fluorene, thus, may be the most likely candidate for product component **A1**. As we stated above, however, without the actual

reference standards of all the methyldibenzo[*a,i*]fluorenes, we cannot designate with any certainty the positions of the methyl groups in components **A1**, **A2**, and **A3**. We can be sure, however, that each is a methyldibenzo[*a,i*]fluorene.

*Dibenzo[*a,g*]fluorenes.* Figure 8 shows the UV spectrum of the M 266 product labelled **B** in Figure 4 and that of a reference standard of dibenzo[*a,g*]fluorene. The UV spectral match confirms the identity of component **B** as dibenzo[*a,g*]fluorene.

Figure 9 displays the UV spectrum of component **B1**, eluting at 47.7 minutes in Figure 4, along with that of the reference standard of dibenzo[*a,g*]fluorene. The small shift toward higher wavelength (in the UV spectrum of component **B1**) again indicates the presence of an alkyl group on the base structure of dibenzo[*a,g*]fluorene. The mass spectrum of component **B1**, shown as an inset in Figure 9, reveals a molecular mass of 280, corresponding to a molecular formula of CH₃-C₂₁H₁₃. This molecular formula, as stated above, is that of a methyldibenzofluorene, and thus the UV and mass spectra of component **B1** confirm the identity of this product as a methyldibenzo[*a,g*]fluorene. It is not possible to determine the exact position of the methyl group on the dibenzo[*a,g*]fluorene base structure since reference standards for all fourteen of the methyl-substituted isomers do not exist. According to the reaction schemes set forth in our companion paper [20], however, there are three positions that each reflect preservation of the two 1-methylnaphthalene units involved in methyldibenzo[*a,g*]fluorene formation: positions 7, 10, and 11. Since component **B1** is a methyldibenzo[*a,g*]fluorene coming from the supercritical 1-methylnaphthalene pyrolysis environment, it is therefore most likely 7-, 10-, or 11-methyldibenzo[*a,g*]fluorene.

*Dibenzo[*a,h*]fluorenes.* Three additional products, **C1**, **C2**, and **C3**, display mass spectra with a major peak of 280 *m/z*, corresponding to a molecular formula of CH₃-C₂₁H₁₃. The product labelled **C2** in Figure 4 has been isolated, by normal-phase HPLC fractionation [32] and reversed-

phase HPLC separation, and analyzed with a fluorescence spectrophotometer. An excitation scan reveals major peaks at the wavelengths 265 nm, 317 nm, and 326 nm—each shifted just 4 nm higher than the major fluorescence excitation peaks published [33] for the unsubstituted dibenzo[*a,h*]fluorene: 261 nm, 313 nm, and 322 nm. An emission scan of component **C2** reveals major peaks at the wavelengths 357 nm, 376 nm, and 396 nm—each shifted just 1 nm higher than the major fluorescence emission peaks published [33] for unsubstituted dibenzo[*a,h*]fluorene: 356 nm, 375 nm, and 395 nm. These uniform bathochromic shifts, relative to the fluorescence spectra of dibenzo[*a,h*]fluorene—of 4 nm, in the excitation spectrum of **C2**, and 1 nm, in the emission spectrum of **C2**—establish that component **C2** is a dibenzo[*a,h*]fluorene with a nonconjugating substituent group such as an alkyl functionality. These fluorescence characteristics of component **C2**—along with its mass spectrum (in the inset of Figure 10), which establishes its molecular formula as $\text{CH}_3\text{-C}_{21}\text{H}_{13}$ —confirm that component **C2** is a methyldibenzo[*a,h*]fluorene.

Figure 10 displays the UV absorbance spectrum of component **C2**, along with that of component **C1**, whose mass spectrum reveals it also to be of molecular mass 280. As Figure 10 illustrates, the UV spectra of components **C1** and **C2** are remarkably similar, separated by only ~2 nm. This similarity in the UV spectra, along with **C1**'s molecular mass of 280, confirms that component **C1** is also a methyldibenzo[*a,h*]fluorene.

An additional molecular mass 280 product, **C3**, has a UV spectrum similar to those of both **C1** and **C2**, with its major peaks shifted ~2 nm higher, relative to those of **C1**. The mass spectrum and UV spectrum of **C3** thus indicate that it is a third methyldibenzo[*a,h*]fluorene product of 1-methylnaphthalene. Reference standards of the fourteen possible methyldibenzo[*a,h*]fluorenes do not exist, so we cannot specify the positions of the methyl substituents in our three methyldibenzo[*a,h*]fluorene products, **C1**, **C2**, and **C3**. However, the

most likely locations of the methyl groups, according to the reaction schemes set forth in our paper [20], are positions 7, 8, 11, and 12.

Benzenoid PAH $C_{22}H_{14}$ PAH. Figure 4 reveals that there are four $C_{22}H_{14}$ PAH products of supercritical 1-methylnaphthalene pyrolysis: dibenz[*a,j*]anthracene, dibenz[*a,h*]-anthracene, picene, and benzo[*c*]chrysene (labelled **D** in Figure 4). Of these four $C_{22}H_{14}$ products, the first three have been previously reported [34-36] as products of either 1-methylnaphthalene or 2-methylnaphthalene pyrolysis or combustion; benzo[*c*]chrysene (component **D**), on the other hand, never has. Therefore the UV spectrum of component **D** is presented in Figure 11, along with that of the reference standard of benzo[*c*]chrysene. The virtual coincidence of the two spectra in Figure 11 establishes the identity of component **D** as benzo[*c*]chrysene. It should be noted that, in addition to the four identified $C_{22}H_{14}$ products, there are eight other possible $C_{22}H_{14}$ isomers—all of whose UV spectra are available to us but none of which are present in our products of 1-methylnaphthalene pyrolysis.

$C_{24}H_{14}$ PAH. PAH of >5 rings have never before been identified as products of 1-methylnaphthalene pyrolysis or combustion. Figure 4 displays two six-ring $C_{24}H_{14}$ PAH, naphtho[2,1-*a*]pyrene (**E**) and naphtho[2,3-*a*]pyrene (**F**), as well as three methyl-substituted counterparts of **E** (**E1**, **E2**, and **E3**). The mass spectra of the products in Figure 4 reveal that, except for the trace level of an as-yet unidentified component, compounds **E** and **F** are the only two $C_{24}H_{14}$ PAH in our 1-methylnaphthalene product mixture—despite the fact that there are over sixty [37,38] possible isomers of $C_{24}H_{14}$ PAH, a third of which are available to us as reference standards. The fact that only two $C_{24}H_{14}$ isomers are observed as products of 1-methylnaphthalene pyrolysis is a direct consequence of the selectivity of the reactions [20] peculiar to our supercritical reaction environment.

The highest-yield product of the $C_{24}H_{14}$ PAH is the 6-ring naphtho[2,1-*a*]pyrene. Figure 12 displays the UV spectrum of the 1-methylnaphthalene pyrolysis product eluting at 63 minutes and labelled **E** in Figure 4, along with that of the reference standard of naphtho[2,1-*a*]pyrene—confirming component **E**'s identity as naphtho[2,1-*a*]pyrene. The large abundance of this particular isomer is most likely due to the fact that it can be formed through various combinations of methyl radicals and 1-methylnaphthalene, two species present in large amounts in this environment [20].

Figure 13 displays the UV spectrum of the reference standard of naphtho[2,1-*a*]pyrene, along with the UV and mass (inset) spectra of the product labelled **E1** in Figure 4. The closely matching features of the UV spectra of component **E1** and naphtho[2,1-*a*]pyrene—combined with the small shift of ~2 nm, evident in the spectrum of **E1**—indicate that **E1** is an alkyl-substituted naphtho[2,1-*a*]pyrene. Since component **E1** elutes at a time in the HPLC/UV/MS during which the solvents methanol and dichloromethane compose the mobile phase, the primary ion in the mass spectrum of the component is at $M+1$, where M is the actual molecular mass. The mass spectrum in the inset of Figure 13 displays a major peak at $M+1 = 317$; thus the molecular mass of component **E1** is $M = 316$, revealing a $CH_3-C_{24}H_{13}$ PAH. The UV and mass spectra presented in Figure 13 thus establish the identity of **E1** as methylnaphtho[2,1-*a*]pyrene.

In total, there are three products in Figure 4, **E1**, **E2**, and **E3**, that display a molecular mass of $M = 316$ and exhibit UV spectra remarkably similar to that of naphtho[2,1-*a*]pyrene—revealing a total of three methylnaphtho[2,1-*a*]pyrenes in the 1-methylnaphthalene product mixture. Analogous to the earlier case of the methyldibenzofluorenes, one must possess standards of all possible methylnaphtho[2,1-*a*]pyrenes in order to establish the exact positions of the methyl groups in product components **E1**, **E2**, and **E3**. Since reference standards of all fourteen methylnaphtho[2,1-*a*]pyrenes do not exist, the exact positions of the methyl substituents

in products **E1**, **E2**, and **E3** remain unknown, but it is certain that they are each a methylnaphtho[2,1-*a*]pyrene.

Figure 14 displays the UV spectrum of the product labelled **F** in Figure 4, along with that of the reference standard of naphtho[2,3-*a*]pyrene. Component **F** is shown in Figure 4 at 74 minutes, eluting off a shoulder of the peak of an unidentified PAH product. Because component **F** is present in small amounts (more than 2 orders of magnitude lower than naphtho[2,1-*a*]pyrene) and because it elutes from the HPLC column so close to another component, some interference occurs in its UV spectrum. The bands present in Figure 14 at wavelengths of 345-416 nm are a result of this interference from the unidentified co-elutant. The UV spectral match, despite the contribution from the co-elutant, confirms the identity of component **F** as naphtho[2,3-*a*]pyrene.

C₂₆H₁₄ PAH. One product from 1-methylnaphthalene supercritical pyrolysis, component **G** in Figure 4, displays a molecular mass of 326, which corresponds to a 7-ring C₂₆H₁₄ PAH. The identity of component **G** is confirmed in Figure 15, which displays the matching UV spectra of component **G** and the reference standard of dibenzo[*cd,lm*]perylene. This is the first time that dibenzo[*cd,lm*]perylene has been identified as a product of 1-methylnaphthalene pyrolysis or combustion. Since no other compound in Figure 4 has a mass spectrum corresponding to a molecular mass of 326, dibenzo[*cd,lm*]perylene is the sole C₂₆H₁₄ PAH product of our 1-methylnaphthalene experiments.

PAH Formation Mechanisms in Supercritical 1-Methylnaphthalene Pyrolysis

The many product PAH of Figure 3 fall into six classes, as listed in Table 1: Class 1, naphthalene and the alkylated naphthalenes, accounting for 46% and 12%, respectively, of the PAH products and eluting in the 13- to 25-minute retention-time range of the HPLC chromatogram of Figure 3; Class 2, the bi-naphthyls, accounting for 39% of the PAH products and eluting from 26 to 38 min; Class 3 (structures shown in blue), the C₂₀H₁₂ 5-ring PAH and

their methyl derivatives, accounting for 0.071% of the PAH products; Class 4 (structures shown in green), the dibenzofluorenes, accounting for 0.86% of the PAH products; Class 5 (structures shown in red), the $C_{22}H_{14}$ 5-ring PAH, accounting for 0.39% of the PAH products; and Class 6 (structures shown in black), the 6-ring and 7-ring PAH, accounting for 0.50% of the PAH products and eluting after 62 minutes. Our Thirty-First International Combustion Symposium paper [20] describes each of the product groups in detail, in addition to the radical reaction pathways leading to their formation in the supercritical 1-methylnaphthalene pyrolysis environment. The key findings of that paper [20] are summarized here in Table 1 and are described in the following. Useful in the ensuing discussion is an awareness of the various bond dissociation energies (BDEs) associated with the 1-methylnaphthalene molecule. The various BDE values [39,40], depicted in Figure 16, show that the methyl C-H bond is the bond of lowest BDE. Therefore, in our analyses of the radical reaction pathways for the 1-methylnaphthalene pyrolysis environment, we presume, as have others [35,41], that the initial source of radicals is homolysis of the methyl C-H bond, to yield 1-naphthylmethyl radical and hydrogen atom.

As shown in Table 1, the first group of supercritical 1-methylnaphthalene pyrolysis products are those of Class 1: naphthalene, 1-ethylnaphthalene, 2-methylnaphthalene, all ten of the dimethylnaphthalenes, and one C_3 -substituted naphthalene. As depicted in Table 1, the Class 1 products result from either displacement of methyl by hydrogen or vice versa. What the structures of the Class 1 products reveal is that within the supercritical 1-methylnaphthalene pyrolysis environment, it is possible to break the methyl C-H bond (BDE, 85.1 kcal/mole [39]), the methyl-aryl C-C bond (BDE, 103.8 kcal/mole [39]), and the aryl C-H bond (BDE, 112.2 kcal/mole [39]). Since we find no single-ring aromatics among our products and since the gaseous hydrocarbon products we observe (90 % methane, 5% ethane, and the balance C_3 to C_4 alkanes, with only a trace of ethylene—and no acetylene) can all come from methyl and

hydrogen—we see that the only kind of bond that appears not to be broken in this reaction environment is the aromatic C-C bond (BDE, 122.3 kcal/mole [40]). We could thus expect the larger aromatic products in this reaction environment to be formed by different combinations of methyl, hydrogen, naphthalene, and 1-methylnaphthalene radicals and molecules—forming bonds in ways that preserve the 2-ring aromatic units of the reacting naphthalene and methylnaphthalene entities.

The first evidence that this hypothesis is indeed the case comes from the structures of the Class 2 products, the bi-naphthyls and methylated bi-naphthyls, the large cluster of peaks between 26 and 38 min in Figure 3. Examples of some of the > 30 Class 2 products are shown in the left-most column of Table 1. As indicated in the middle column of Table 1, the Class 2 products are formed by displacement of 1-methylnaphthalene's methyl or one of its hydrogens by naphthylmethyl, methylnaphthyl, or naphthyl radical. What we see from the structures of the Class 2 products is that the two-ring naphthalene units stay intact as the various methyl and hydrogen displacements take place on the periphery of the structure.

The next group of 1-methylnaphthalene products in Table 1 are those of Class 3, the five-ring $C_{20}H_{12}$ PAH. These Class 3 products result from the cyclodehydrogenation of the Class 2 products, as illustrated in Table 1. No breaking of the aromatic C-C bond is involved in the process, so the intactness of the two participating 2-ring naphthalene units is preserved in the resulting five-ring fused PAH structures. We know from our HPLC/UV/MS analyses that other $C_{20}H_{12}$ isomers of the Class 3 products, such as the two compounds shown in the right-most column of Table 1 (in the Class 3 section), are not produced in the supercritical 1-methylnaphthalene reaction environment, and their absence is not a surprise since they cannot be formed from two naphthalene units in a way that would preserve the intactness of the naphthalene units.

The second group of five-ring products of 1-methylnaphthalene, also pictured in Table 1, are those of Class 4, the $C_{21}H_{14}$ dibenzofluorenes and their methyl derivatives. As shown in Table 1, the dibenzofluorenes are formed by 1-naphthylmethyl displacement of an aryl H of either naphthalene or a methylnaphthalene, followed by dehydrogenation. As in the case of the Class 3 products, the structures of the $C_{21}H_{14}$ PAH of Class 4 reflect the intactness of the two naphthalene units involved in their construction, and no $C_{21}H_{14}$ isomers that involve other building units such as 1-ring/3-ring combinations are observed. The Class 4 products exhibit an additional level of selectivity in that: $C_{21}H_{14}$ PAH whose formation would require 2-naphthylmethyl radical addition to a “2” position of naphthalene are not made in this 1-methylnaphthalene reaction environment, in which 1-naphthylmethyl would be in much greater abundance than its “2” counterpart.

The third group of five-ring products of supercritical 1-methylnaphthalene pyrolysis, also listed in Table 1, are the $C_{22}H_{14}$ PAH composing Class 5. As shown in Table 1, these $C_{22}H_{14}$ PAH are produced by the addition of 1-naphthylmethyl radical to either 1-methylnaphthalene or 2-methylnaphthalene, followed by dehydrogenation. As in the case of the other Classes of five-ring products, we see that the four Class 5 $C_{22}H_{14}$ products all preserve the intactness of the two 2-ring naphthalene units involved in their formation. Because our HPLC/UV/MS technique enables us to see which isomers of the 12 possible $C_{22}H_{14}$ PAH are present as well as which are not, we can see that the $C_{22}H_{14}$ Class 5 products exhibit several degrees of selectivity: (1) $C_{22}H_{14}$ PAH whose structures do not contain two intact naphthalene units are not observed. (2) $C_{22}H_{14}$ PAH whose construction involves the combination of a 2-naphthylmethyl radical and a 2-methylnaphthalene molecule—but no involvement of the “1” counterparts—are not observed. (3) For a given sequence of steps, products constructed from 1-naphthylmethyl radical and 1-methylnaphthalene molecule are produced in higher abundance than are those constructed from 1-naphthylmethyl radical and 2-methylnaphthalene.

Product selectivity is particularly evident among the last set of 1-methylnaphthalene products listed in Table 1, those comprising Class 6: the 6- and 7-ring PAH eluting between 63 and 80 min in Figure 3, whose structures are shown in black. None of the Class 6 products has ever before been reported as a product of 1-methylnaphthalene pyrolysis or combustion.

As Figure 3 reveals, the highest-yield Class 6 product is the $C_{24}H_{14}$ naphtho[2,1-*a*]pyrene, whose formation, we propose, occurs as depicted in the top row of the second column of Table 1, in the Class 6 section. As shown in the second row of the same column, naphtho[2,3-*a*]pyrene, the other $C_{24}H_{14}$ product we observe, would form according to the same sequence, but with the initial methyl additions occurring to the methyl group of 2-methylnaphthalene instead of to 1-methylnaphthalene. The yield of naphtho[2,3-*a*]pyrene is more than two orders of magnitude lower than that of naphtho[2,1-*a*]pyrene—reflecting the much lower level of 2-methylnaphthalene in our system, relative to 1-methylnaphthalene. We know from our HPLC/UV/MS analyses that only one other $C_{24}H_{14}$ PAH (as yet unidentified) exists among our 1-methylnaphthalene products, and that one is also only in trace levels.

The fact that one particular 6-ring compound, naphtho[2,1-*a*]pyrene, is in such high yield (comparable to those of some of the more abundant di-methylnaphthalenes) is truly remarkable, especially when one considers that naphtho[2,1-*a*]pyrene belongs to the $C_{24}H_{14}$ PAH family of which there are 65 possible isomers [37]. Once again we witness the extreme selectivity of the products formed in the supercritical 1-methylnaphthalene pyrolysis reaction environment. Our paper [20] provides the details as to why the other $C_{24}H_{14}$ PAH are not formed in this reaction environment; some examples are highlighted here, in the last column of Table 1, under the Class 6 section. The long and short of it is that—just as we observed for the 5-ring PAH products—the 6-ring products which are formed are those whose structures preserve the intactness of the parent

two 2-ring naphthalene units, whose reaction pathways involve the species most abundant in the reaction environment, and whose formation involves bond breakage at the sites of lowest BDE.

The bottom row of Table 1 reveals the remaining Class 6 product: the 7-ring dibenzo[*cd,lm*]perylene, whose formation pathway runs along the same lines as those for the 6-ring PAH but with two extra methylations required. As with the 5- and 6-ring PAH, a high degree of selectivity is exhibited by the 7-ring PAH, as dibenzo[*cd,lm*]perylene is the only $C_{26}H_{14}$ PAH product detected in the supercritical 1-methylnaphthalene pyrolysis products.

In addition to the 2- to 7-ring PAH products listed in Table 1, Figure 3 shows seven unidentified peaks: six labelled “402” and one labelled “426,” in accordance with the molecular masses determined from the mass spectra for those components. In order to learn more about these 8- and 9-ring products (which may be key precursors to carbonaceous solids), the product mixture portrayed in Figure 3 has been subjected to another HPLC/UV/MS analysis employing the solvents methanol and dichloromethane, which optimize HPLC separation of the high-ring-number PAH. The end segment of the resulting HPLC chromatogram [42] is pictured in Figure 17, which shows two of the Class 6 products from Figure 3 as well as eleven unsubstituted 8- and 9-ring PAH products: six 8-ring $C_{32}H_{18}$ of molecular mass 402 and five 9-ring $C_{34}H_{18}$ of molecular mass 426. There are also five molecular-mass 416 products which, we know from their mass and UV spectra, are methylated versions of two of the 8-ring $C_{32}H_{18}$ products.

In the supercritical 1-methylnaphthalene pyrolysis environment, the 8-ring $C_{32}H_{18}$ PAH can be constructed from 1-naphthylmethyl radical reacting with naphthalene and 1-methylnaphthalene; the 9-ring $C_{34}H_{18}$ PAH can be constructed from 1-naphthylmethyl radical, methyl, and two 1-methylnaphthalenes. Of the 287 theoretically possible benzenoid $C_{32}H_{18}$ PAH and the 333 theoretically possible benzenoid $C_{34}H_{18}$ PAH [43], there are, respectively, only 13 [44-49] and 12 isomers [49-53] for which UV spectra have been published, and none of these

published UV spectra match any of the spectra of our $C_{32}H_{18}$ and $C_{34}H_{18}$ 1-methylnaphthalene products. Even if one imposes the restriction—based on the findings of our 2- to 7-ring products—that the 8- and 9-ring PAH products must reflect the preservation of the three 2-ring naphthalene units that could be involved in their construction, the field of possible $C_{32}H_{18}$ and $C_{34}H_{18}$ benzenoid PAH candidates is only “narrowed down” to, respectively, 83 and 189 isomers—still some rather daunting numbers since only 6 of the 83 and 2 of the 189 have published UV spectra.

Nevertheless, the HPLC/UV/MS instrument, in conjunction with Annellation Theory [25,49], has enabled us to identify the latest-eluting molecular-mass 426 component in Figure 17. The very long HPLC elution time (174 min) itself provides a very important clue to the identity of this product component: because of its very long elution time, this PAH product has to be planar and has to have a high length-to-breadth ratio [54-56]. This late-eluting $C_{34}H_{18}$ PAH product, we believe, is benzo[*cd*]phenanthro[1,2,3-*lm*]perylene, whose structure is shown in red in Figures 18 and 19, along with the UV spectral evidence supporting this product’s identification. No reference standard or published UV spectrum of benzo[*cd*]phenanthro[1,2,3-*lm*]perylene exists, so—unlike Figures 11, 12, 14, and 15, which show the UV spectra of the unsubstituted benzenoid PAH product components with those of their respective reference standards—Figures 18 and 19 show the UV spectrum of the $C_{34}H_{18}$ product component eluting at 174 min (which we are deducing to be benzo[*cd*]phenanthro[1,2,3-*lm*]perylene), along with the published UV spectra of two of benzo[*cd*]phenanthro[1,2,3-*lm*]perylene’s benzologues: one with one ring less, the $C_{30}H_{16}$ benzo[*cd*]naphtho[1,2,3-*lm*]perylene [25,51], shown in black in Figure 18; and one with one ring more, the $C_{36}H_{18}$ teropyrene [57], shown in black in Figure 19. The extreme similarity between the two spectra of Figure 18 establishes that the structure of the $C_{34}H_{18}$ product component eluting at 174 min in Figure 17 has to resemble very closely the structure of

benzo[*cd*]naphtho[1,2,3-*lm*]perylene, the C₃₀H₁₆ shown in black in Figure 18. The line of reasoning leading to our deduction of the exact structure of the C₃₄H₁₈ product is detailed in the following.

Consistent with the similarities of the three molecular structures drawn in Figures 18 and 19, all three of the UV spectra in the two figures exhibit the same basic shapes and patterns, especially in the relative heights of the peaks in the *p* band (the three highest-wavelength peaks). The three molecules are not the same, however, so there are differences between the spectra in Figures 18 and 19, primarily in the positions (wavelengths) of the various spectral peaks: the red spectrum of the 9-ring compound in Figure 18 is very similar (in the β and *p* bands) to the black spectrum of the 8-ring compound, but there are some differences in the β' band; the black spectrum of the 10-ring compound in Figure 19 is shifted substantially, relative to the red spectrum of the 9-ring compound. The spectral similarities and differences among the benzologues of Figures 18 and 19 are fully consistent with the assignment of the 9-ring product's identity as benzo[*cd*]phenanthro[1,2,3-*lm*]perylene, however, and can be explained by Annellation Theory [25,49,58,59], as detailed below.

One tenet of Annellation Theory [25,49,58,59] is that the addition of a ring to a bay region of a PAH molecule causes the overall appearance of the UV spectrum to be preserved but shifts the spectrum to higher wavelengths (~10 nm for the β band and 10s of nm for the *p* band). The 9- and 10-ring PAH of Figure 19 conform exactly to this behavior. The structure of teropyrene differs from that of benzo[*cd*]phenanthro[1,2,3-*lm*]perylene by the addition of a ring to a bay region, and its spectrum, relative to that of the 9-ring benzologue, is shifted ~15 nm in the β band and 50-60 nm in the *p* band.

A second tenet of Annellation Theory [25,49,58,59] states that when addition of a ring to a PAH molecule (a) occurs to a ring that shares an aromatic sextet with a neighboring ring and (b)

results in the addition of an aromatic sextet, the effect on the p band of the UV spectrum is extremely minimal (but the β and β' bands may be shifted). The 8- and 9-ring PAH of Figure 18 conform exactly to this behavior. The structure of benzo[*cd*]phenanthro[1,2,3-*lm*]perylene differs from that of benzo[*cd*]naphtho[1,2,3-*lm*]perylene by the addition of an aromatic sextet to a ring that shares an aromatic sextet with a neighboring ring, and the p bands of the UV spectra of the two compounds are extremely similar, both in shape and in position. The β' band of the 9-ring compound's spectrum is shifted ~4 nm to the right, relative to that of the 8-ring compound.

In order to confirm that the 9-ring product component eluting at 174 min in Figure 17 is in fact benzo[*cd*]phenanthro[1,2,3-*lm*]perylene and cannot be any other $C_{34}H_{18}$ benzologue of benzo[*cd*]naphtho[1,2,3-*lm*]perylene (the 8-ring structure of Figure 18), we consider the structures of all of the benzenoid molecules of formula $C_{34}H_{18}$ that can result by addition of a ring to benzo[*cd*]naphtho[1,2,3-*lm*]perylene. The nine possible $C_{34}H_{18}$ structures are shown in Figure 20, along with that of benzo[*cd*]naphtho[1,2,3-*lm*]perylene itself, the “parent” 8-ring compound in the center of Figure 20. Immediately we can see that five of the nine possibilities—those in green, resulting from ring fusion to the *e*, *i*, *p*, *t*, or *x* sides of benzo[*cd*]naphtho[1,2,3-*lm*]perylene—cannot be our 9-ring $C_{34}H_{18}$ product since each of these five has a “cove” region that makes the molecular structure nonplanar [25]. The nonplanarity would cause these species to elute much earlier in Figure 17 than the 174 min of our $C_{34}H_{18}$ product. Nonplanarity also causes broadening of bands in the UV spectra—as well as attenuation of spectral peaks and raising of spectral valleys [25]—so the $C_{34}H_{18}$ product component spectrum in Figures 18 and 19 could not correspond to any of the five nonplanar structures (in green) in Figure 20.

To assess the remaining four possible $C_{34}H_{18}$ PAH of Figure 20, we next employ a corollary to the second tenet of Annellation Theory [25,49,58,59], which states that if ring addition to a ring that shares an aromatic sextet with a neighboring ring does not result in the addition of a sextet

(i.e., a violation of condition (b) in the second tenet above), then the UV spectrum is altered substantially: the *p* band is shifted 10s of nm; the *β* band shifts and is altered in shape. In Figure 20, fusion of a ring to the *o* side of benzo[*cd*]naphtho[1,2,3-*lm*]perylene corresponds to just such a case, so the blue structure at the top of Figure 20 is eliminated as a candidate for our C₃₄H₁₈ product eluting at 174 min in Figure 17 (because the *p*-band of our C₃₄H₁₈ product is definitely not shifted 10s of nm higher than the *p*-band of the 8-ring compound in Figure 18).

In our consideration of the final three C₃₄H₁₈ candidates in Figure 20, we turn to a third tenet of Annellation Theory [25,49,58,59], which states that addition of a ring to an aromatic sextet preserves the basic appearance of the UV spectrum but shifts it to substantially higher wavelengths (by ~30 nm for the highest-wavelength peak of the *p* band), provided that the resulting molecule has the same number of aromatic sextets as the parent molecule. Fusion of a ring to either the *a* or *b* side of benzo[*cd*]naphtho[1,2,3-*lm*]perylene exemplifies this case, so the UV spectra of the two structures shown in turquoise at the bottom of Figure 20 would be substantially different from that of benzo[*cd*]naphtho[1,2,3-*lm*]perylene. The third tenet of Annellation Theory thus rules the two turquoise structures out as possible candidates for the C₃₄H₁₈ product eluting at 174 min in Figure 17.

We see that the only one of the nine C₃₄H₁₈ possibilities that meets all of the criteria—molecular formula C₃₄H₁₈, planarity, high length-to-breadth ratio, UV spectrum similar to that of the 8-ring benzologue and consistency with the tenets of Annellation Theory—is benzo[*cd*]phenanthro[1,2,3-*lm*]perylene, shown in red in Figures 18, 19, and 20. We also note that benzo[*cd*]phenanthro[1,2,3-*lm*]perylene's structure reflects the preservation of three intact 2-ring naphthalene units—just as the structures of the 5- to 7-ring products in Figure 3 and Table 1 reflect the preservation of two intact 2-ring naphthalene units. Benzo[*cd*]phenanthro[1,2,3-*lm*]perylene is thus the C₃₄H₁₈ PAH product of supercritical 1-methylnaphthalene pyrolysis that

elutes at 174 min in Figure 17. This PAH has never before been identified as a product of any fuel under any condition. In fact—except for our DURIP grant’s Final Performance Report [60] reporting on the same finding— benzo[*cd*]phenanthro[1,2,3-*lm*]perylene has never before been reported in the scientific literature. The paper we are currently preparing for publication [42] will be the first documentation of this molecule’s existence.

Figure 21 presents the reaction scheme [42] for the formation of benzo[*cd*]phenanthro[1,2,3-*lm*]perylene in the supercritical 1-methylnaphthalene pyrolysis environment. Methylation of the methyl group of 1-methylnaphthalene forms 1-ethylnaphthalene (a product in Figure 3), which then reacts with two 1-naphthylmethyl radicals, as shown in Figure 21, and undergoes a series of dehydrogenation and ring-closure steps to form benzo[*cd*]phenanthro[1,2,3-*lm*]perylene. Just as the reaction schemes of Table 1—forming the 5-, 6-, and 7-ring products of Figure 3—involve the combination of two naphthalene or 1-methylnaphthalene molecules or radicals and methyl, the scheme to form the 9-ring benzo[*cd*]phenanthro[1,2,3-*lm*]perylene in Figure 21 involves combination of three naphthalene or 1-methylnaphthalene molecules or radicals and methyl. We expect that the other C₃₄H₁₈ products of Figure 17, not yet identified, would be formed by reactions very similar to the scheme of Figure 21 but with aryl-alkyl bonds forming at different aryl positions during the sequence, resulting in different isomeric configurations of 9-ring structures.

The fact that—out of the hundreds of possible 8- and 9-ring PAH—only six C₃₂H₁₈ and five C₃₄H₁₈ isomers exhibit prominence in Figure 17 suggests that a high degree of product selectivity is in effect for these 8- and 9-ring products, just as it has been demonstrated in the 5-, 6-, and 7-ring PAH products of supercritical 1-methylnaphthalene pyrolysis. Even though the exact identities of most of these 8- and 9-ring products have not yet been determined, their presence, along with their suggested selectivity, serve as evidence that the types of reaction mechanisms

outlined in Table 1—for the combination of two naphthalene and methylnaphthalene entities in the formation of 5- to 7-ring PAH—also apply to the combination of three and more such entities in the formation of larger-ring-number PAH and eventually carbonaceous solids.

Model Fuel Experiments with Toluene

The results described above illustrate the usefulness of the model fuel experiments, in conjunction with the HPLC/UV/MS analysis technique, in discerning the structures of PAH products and determining the reaction pathways responsible for PAH formation from the 2-ring aromatic jet fuel component 1-methylnaphthalene. We now report the results of applying this same experiments/analysis technique combination to the 1-ring aromatic jet fuel component toluene (critical temperature, 319 °C; critical pressure, 41 atm).

Figure 22 presents the HPLC chromatogram [17] of supercritical toluene pyrolysis products from experiments in the reactor of Figure 1, at conditions of 535 °C, 100 atm, and 140 sec. Since large PAH can be precursors [16] to carbonaceous solids in the supercritical fuel pyrolysis environment, of particular interest is the set of six 8-ring $C_{28}H_{14}$ PAH, whose structures are shown in red in Figure 22 as well as in Table 2, a listing of all the possible $C_{28}H_{14}$ benzenoid PAH. Two of these six $C_{28}H_{14}$ products, benzo[*a*]coronene and benzo[*pqr*]naphtho[8,1,2-*bcd*]perylene, the first two entries of Table 2, have been identified [61] by matching the UV spectra of the product components with those of the specially synthesized [51,62-64] reference standards in our collection. The UV spectral matches confirming these two products' identifications appear in Figures 23 and 24

The next two entries of Table 2, phenanthro[5,4,3,2-*efghi*]perylene and benzo[*cd*]naphtho[8,1,2,3-*fghi*]perylene, we have identified [61] by establishing the components' molecular formula ($C_{28}H_{14}$) from their mass spectra and then matching the components' UV spectra with those published [65-67] for the respective PAH reference standards. The UV spectra

confirming these two products' identities appear in Figures 25 and 26. As Figure 22 reveals, benzo[*a*]coronene, phenanthro[5,4,3,2-*efghi*]perylene, and benzo[*cd*]naphtho[8,1,2,3-*fghi*]perylene elute very closely together, so the UV spectrum of the product component in Figure 25 shows interference from a UV spectral peak of benzo[*a*]coronene, and the UV spectrum of the product component in Figure 26 shows interference from the UV spectrum of phenanthro[5,4,3,2-*efghi*]perylene. Once these interferences from co-eluting compounds are taken into account, however, the UV spectra of Figures 25 and 26 confirm the two C₂₈H₁₄ products' identities as phenanthro[5,4,3,2-*efghi*]perylene and benzo[*cd*]naphtho[8,1,2,3-*fghi*]perylene, respectively.

Reference standards do not exist for the remaining two C₂₈H₁₄ products of Figure 22, benzo[*ghi*]naphtho[8,1,2-*bcd*]perylene and tribenzo[*cd,ghi,lm*]perylene, but we have been able to establish these two products' identities through extensive analyses [58,68] of the components' HPLC retention time data (which relate to molecular length-to-breadth ratios), mass spectra, and UV spectra, as well as Annellation Theory—just as we have illustrated in the previous section for the identification of the C₃₄H₁₈ benzo[*cd*]phenanthro[1,2,3-*lm*]perylene as a product of the supercritical pyrolysis of 1-methylnaphthalene. Neither of these two C₂₈H₁₄ products, benzo[*ghi*]naphtho[8,1,2-*bcd*]perylene or tribenzo[*cd,ghi,lm*]perylene (the fifth and sixth entries of Table 2), has ever before been identified as a product of fuel pyrolysis or combustion, and since reference standards of neither exist, the analyses of the chromatographic and spectral evidence documenting each of these two products' identities are very extensive and appear in two *Journal of Chromatography A* papers [58,68], one for each compound. Extracted from the first paper [58], Figure 27 shows, in part c, the UV spectrum of the supercritical toluene pyrolysis product component deduced to be benzo[*ghi*]naphtho[8,1,2-*bcd*]perylene—along with the UV spectra, in parts a and b [69], of two related compounds used to deduce benzo[*ghi*]naphtho[8,1,2-*bcd*]perylene's identity. Extracted from the second paper [68], Figure 28 shows, in part b, the UV

spectrum of the supercritical toluene pyrolysis product component deduced to be tribenzo[*cd,ghi,lm*]perylene—along with the UV spectra, in parts a and c [49], of two related compounds used to deduce tribenzo[*cd,ghi,lm*]perylene's identity.

As in the case of the 1-methylnaphthalene work, the HPLC/UV/MS instrument has enabled us to determine not only which isomers of a given PAH family are products of supercritical toluene pyrolysis but also those that are not. In the case of the $C_{28}H_{14}$ PAH, we have been able to establish that bisanthene, the second-to-last $C_{28}H_{14}$ benzenoid PAH listed in Table 2, is not a product of supercritical toluene pyrolysis, as its published UV spectrum [49] does not match the UV spectrum of any of the six $C_{28}H_{14}$ components in the toluene product mixture. In addition, Annellation Theory has permitted us to establish [58,68] from the predicted UV spectrum, that naphthaceno[3,4,5,6,7-*defghij*]naphthacene, the last entry of Table 2, is also not among the supercritical toluene pyrolysis products.

Figure 29, extracted from our reaction mechanisms paper [17], illustrates how the six $C_{28}H_{14}$ products in Figure 22 and Table 2 are formed in the supercritical toluene pyrolysis environment. As in the case of 1-methylnaphthalene, the products of supercritical toluene pyrolysis show that the aromatic C-C bond is not broken in this reaction environment; so, as Figure 29 shows, the PAH are “built” from sequential additions of benzyl, methyl, and/or phenyl radicals—all plentiful in the toluene pyrolysis environment—followed by dehydrogenation. Just as the major building blocks for PAH formation from supercritical 1-methylnaphthalene pyrolysis have been shown [20] to be 1-naphthylmethyl radical, methyl radical, 1-methylnaphthalene, and naphthalene—Figure 29 reveals that the building blocks for PAH formation from supercritical toluene pyrolysis are the exact analogues: benzyl radical, methyl radical, toluene, and benzene (or phenyl radical). Another similarity in the results for the two aromatic fuels is that—just as the HPLC/UV/MS analyses of the 1-methylnaphthalene products have helped to provide mechanistic insight into

why certain 5- to 7-ring PAH are formed and why others are not [20]—so have the HPLC/UV/MS analyses of the toluene products helped to provide mechanistic insight into why certain PAH are formed and others are not in the supercritical toluene pyrolysis environment: Figure 29 shows that all six of the $C_{28}H_{14}$ products of supercritical toluene pyrolysis are produced via pathways that involve intermediates that are fully aromatic benzenoid structures that themselves are observed products (shown in bold print) in Figure 22. Figure 30 demonstrates that attempts to form—from the benzyl, methyl, and phenyl building blocks in our system—the two $C_{28}H_{14}$ PAH of Table 2 that are known not to be among our products would involve not-fully-aromatic intermediates that we know from our HPLC/UV/MS analyses are also not present in the product mixture. There are thus mechanistic reasons why certain large PAH are made and why certain others are not in the supercritical toluene pyrolysis environment—just as we have seen for the supercritical 1-methylnaphthalene pyrolysis environment.

The reaction mechanisms of Figure 29 can also account for the relative amounts of the six observed $C_{28}H_{14}$ products of supercritical toluene pyrolysis. Since average UV absorbance over the range 190-520 nm is the y-axis of the HPLC chromatogram in Figure 22, chromatographic peak area is directly proportional to mass [70] for the six $C_{28}H_{14}$ PAH products. Although co-elution inhibits accurate quantification of some of the $C_{28}H_{14}$ PAH isomers, it is still clear that tribenzo[*cd,ghi,lm*]perylene, the latest-eluting $C_{28}H_{14}$ PAH in Figure 22 and the sixth entry of Table 2, is the lowest-yield $C_{28}H_{14}$ PAH product and that benzo[*ghi*]naphtho[8,1,2-*bcd*]perylene, the fifth entry in Table 2, is by far the highest-yield $C_{28}H_{14}$ PAH product of supercritical toluene pyrolysis at 535 °C and 100 atm. These two observations can be partially explained by the facts that dibenzo[*cd,lm*]perylene, the precursor to tribenzo[*cd,ghi,lm*]perylene in Figure 29, is present only in trace amounts, the lowest amount of any of the $C_{28}H_{14}$ precursors in Figure 29—and that benzo[*a*]pyrene, the precursor to benzo[*ghi*]naphtho[8,1,2-*bcd*]perylene in Figure 29, is the

highest-yield precursor to a $C_{28}H_{14}$ PAH in Figure 29. It is also the case, however, that benzo[ghi]naphtho[8,1,2-*bcd*]perylene is the only one of the six $C_{28}H_{14}$ PAH products in Figure 29 that is unlikely to participate in further molecular growth reaction sequences of the types A and B illustrated in Figure 29. All five of the other $C_{28}H_{14}$ PAH products in Figure 29 contain bay regions and—through addition of methyl and benzyl, in a type A reaction, or of phenyl, in a type B reaction—would yield larger PAH that do not contain any cove or fjord regions, which introduce molecular strain and lead to nonplanar structures. For benzo[ghi]naphtho[8,1,2-*bcd*]perylene, on the other hand, addition of methyl and benzyl or phenyl would yield PAH with a cove region, and the associated molecular strain would cause such products to be disfavored. (Of the forty-four PAH identified so far [58,61,68] in the products of supercritical toluene pyrolysis, none contains a cove or fjord region.) Therefore as a consequence of the higher abundance of its precursor species and the preclusion of its structure from participating in the benzyl-, methyl-, and phenyl-addition reactions prevalent in the supercritical toluene pyrolysis environment, benzo[ghi]naphtho[8,1,2-*bcd*]perylene is the most abundant $C_{28}H_{14}$ PAH in the product mixture.

Evidence that the other five $C_{28}H_{14}$ PAH products of supercritical toluene pyrolysis do participate in further molecular growth reactions of the types A and B is found in Figure 31, the end portion of the supercritical toluene pyrolysis products' HPLC chromatogram generated from the same alternate HPLC solvent program responsible for the 1-methylnaphthalene products chromatogram excerpted in Figure 17. The chromatogram reveals the presence of seven 10-ring $C_{34}H_{16}$ PAH and three 11-ring $C_{36}H_{16}$ PAH whose structures have not yet been determined. What we can say now, however, is that the $C_{28}H_{14}$ products in Figures 22 and 29 are likely key intermediates in the formation of these 10- and 11-ring PAH. The 10-ring $C_{34}H_{16}$ PAH can result from phenyl addition to $C_{28}H_{14}$ PAH (the type of reaction labelled "B" in Figure 29), followed by dehydrogenation. The 11-ring $C_{36}H_{16}$ PAH can result from methyl and benzyl addition to $C_{28}H_{14}$

PAH (the type of reaction sequence labelled “A” in Figure 29), followed by dehydrogenation. We thus see that the types of reaction mechanisms we have determined for the 2- to 8-ring product PAH in Figure 29 are also applicable to the formation of 10- and 11-ring PAH products of supercritical toluene pyrolysis—and by extension, likely relevant to the formation of carbonaceous solids.

Model Fuel Experiments with Methylcyclohexane

The results just above apply to the single-ring aromatic jet fuel component toluene, which is also the main dehydrogenation product of the endothermic fuel methylcyclohexane. Supercritical pyrolysis experiments have also been conducted with methylcyclohexane itself (critical temperature, 299 °C; critical pressure, 34 atm). The effects of pressure, temperature, and residence time on PAH production from methylcyclohexane are discussed in the Final Technical Report [71] of our previous grant. We focus here on how the product PAH are formed.

Figure 32 presents the HPLC chromatogram of the products of methylcyclohexane pyrolysis at 570 °C, 100 atm, and 140 sec. One-ring and two-ring aromatic products are lost by evaporation during the solvent-exchange procedure that prepares the product sample for HPLC analysis, so the one- and two-ring aromatic products are under-represented in Figure 32. GC-MS analysis of the products (not solvent-exchanged) reveals that toluene is by far the highest-yield aromatic product of methylcyclohexane pyrolysis at this condition. It is not a surprise, therefore, that the products of methylcyclohexane in Figure 32 are very similar to those of toluene in Figure 22. In fact, except for tribenzo[*cd,ghi,lm*]perylene (which is present in the toluene products in only trace amounts), all of the 32 unsubstituted PAH products of toluene in Figure 22 are also present in the methylcyclohexane products of Figure 32. Methylcyclohexane produces only three additional unsubstituted PAH of 5 to 7 rings that have not been detected in the toluene products—dibenzo[*a,h*]anthracene, dibenzo[*b,k*]fluoranthene, and naphtho[2,3-*k*]fluoranthene—in addition

to higher quantities of alkylated PAH. Dibenzo[*cd,lm*]perylene, which is present in the toluene products in only trace amounts, is present in measurable amounts in the methylcyclohexane products.

The fact that the methylcyclohexane PAH product distribution in Figure 32 resembles so closely that of toluene in Figure 22—coupled with the fact that toluene is the major aromatic product of methylcyclohexane in this reaction environment—suggests that the basic radical reaction pathways to large PAH, outlined in Figure 29 for toluene, also hold for the supercritical pyrolysis of methylcyclohexane. Analysis of the gas-phase products of methylcyclohexane shows that methane is the most abundant gaseous product, so methyl radicals would be abundant in the methylcyclohexane reaction environment, contributing to the large levels of methylated PAH products observed in Figure 32. Other small hydrocarbon products such as ethane and propane may also contribute to the alkylation in the PAH products of methylcyclohexane.

Analysis of Stressed Fischer-Tropsch Synthetic Jet Fuel S-8 from UTRC

In our communications [72] with Dr. Tim Edwards at AFRL, we have learned that the Air Force is interested in a certain Fischer-Tropsch synthetic jet fuel S-8, for potential use in future high-speed aircraft. This fuel—which is composed of a mixture of C₁₀ to C₁₅ alkanes, both straight-chain (*n*-alkanes) as well as branched-chain (*iso*-alkanes)—has apparently formed higher-than-expected levels of carbonaceous solids in tests performed at UTRC. At Dr. Edwards' instigation, Dr. He Huang of UTRC sent us a set of samples from this fuel that had been “stressed” at supercritical conditions of 42 atm and temperatures of 590 to 710 °C. We have subjected three of these samples (635 °C, 674 °C, and 710 °C) to HPLC analysis—two of them to HPLC/UV only; the third to HPLC/UV/MS.

The chromatograms from our HPLC/UV/MS analyses—employing both the main and alternate solvent programs—of the 710-°C, 42-atm stressed S-8 fuel sample appear in Figures 33

and 34, respectively. The figures reveal that the stressed Fischer-Tropsch fuel sample contains over 80 identified PAH of up to ten fused aromatic rings. Except for our own supercritical pyrolysis experiments [32] with model alkane fuels, most of the PAH of > 6 rings in Figures 33 and 34 have never before been identified as products of alkane pyrolysis or combustion. As in the cases already discussed of the products of the model fuels 1-methylnaphthalene, toluene, and methylcyclohexane, most of the identifications of the Fischer-Tropsch synthetic jet fuel products have come from matching UV spectra with those of authentic reference standards or with those published for the reference standards. The structural determinations of three of the products in Figures 33 and 34—benz[*a*]anthanthrene, tribenzo[*cd,ghi,lm*]perylene [68], and dibenzo[*e,ghi*]naphtho[8,1,2-*klm*]perylene—have employed Annellation Theory, in conjunction with the UV spectra of appropriate benzologues, since reference standards do not exist and UV spectra have never before been published for those compounds.

Identifications [73,74] of others of the products in Figures 33 and 34—benzo[*cd*]naphtho[1,2,3-*lm*]perylene, dibenzo[*b,ghi*]perylene, 8H-dibenzo[*a,jk*]pyrene, and benzo[*pqr*]dinaphtho[8,1,2-*bcd:2',1',8'-lmn*]perylene—have required allowances for solvent effects in the UV spectra of the product components. Figure 35 presents the mass spectral and UV spectral evidence [73] supporting the identification of the first one of these four, the eight-ring C₃₀H₁₆ benzo[*cd*]naphtho[1,2,3-*lm*]perylene, the latest-eluting identified compound in Figure 33 and the component eluting at 141 min in Figure 34. Figure 35a establishes that the component eluting at 141 min in Figure 34 is of molecular mass 376 and molecular formula C₃₀H₁₆. Figure 35b shows the UV spectrum of the product component and that published [25,51] for the reference standard of benzo[*cd*]naphtho[1,2,3-*lm*]perylene. The two spectra in Figure 35b match well, confirming the identity of this product component as benzo[*cd*]naphtho[1,2,3-*lm*]perylene. This is the first time that this C₃₀H₁₆ product has ever been identified as a product of the pyrolysis

or combustion of any fuel [73]. Although it is present in small amounts, its large molecular size and high length-to-breadth ratio may make it of particular significance in the formation of carbonaceous solids. Since this 8-ring PAH and several other high length-to-breadth-ratio products in Figures 33 and 34 do not appear in our supercritical pyrolysis products from our model aromatic fuels, we suspect that several of these products may be peculiar to the long-chain alkane nature of the Fischer-Tropsch synthetic jet fuel from which these products came. Because the UTRC tests have shown that this Fischer-Tropsch synthetic jet fuel is particularly prone to forming carbonaceous solids [72], supercritical pyrolysis experiments with representative alkanes are a major focus of our work on the AFOSR grant that has succeeded the one covered in the present report. It is anticipated that the model fuel experiments and HPLC/UV/MS analyses will play a major role in product identification and reaction mechanism determination for the alkane fuels, just as they have already been shown to do in the cases of the model fuels examined so far.

Executive Summary

Summary of Results

Supercritical pyrolysis experiments with the model fuel 1-methylnaphthalene and analysis of the products by high-pressure liquid chromatography with diode-array ultraviolet-visible absorbance detection and mass spectrometric detection (HPLC/UV/MS) have led to the identification of 38 individual 2- to 7-ring PAH—sixteen of which have never before been reported as products of 1-methylnaphthalene pyrolysis or combustion. The absence, among the reaction products, of single-ring aromatics and acetylene indicates that there is no aromatic ring rupture in this reaction environment, and the structures of each of the 5- to 7-ring PAH products reveal the intactness of the two 2-ring naphthalene units required in their construction. Proposed reaction pathways [20] involving species plentiful in the reaction environment—1-

naphthylmethyl radical, methyl radical, 1-methylnaphthalene, naphthalene, and 2-methylnaphthalene—account for the formation of the observed 5- to 7-ring PAH products. These reaction pathways, along with consideration of bond dissociation energies and relative abundances of reactant species, account for the extremely high product selectivity exhibited by the observed product PAH. The detection, among the supercritical 1-methylnaphthalene pyrolysis products, of six 8-ring $C_{32}H_{18}$ PAH and five $C_{34}H_{18}$ 9-ring PAH—each requiring construction from three naphthalene or methylnaphthalene units—provides evidence that the types of reaction mechanisms we have devised for the combination of two naphthalene entities to form the 5- to 7-ring PAH products also apply to the combination of three and more such entities in the formation of larger-ring-number PAH and eventually carbonaceous solids. HPLC/UV/MS analysis, in conjunction with Annellation Theory, has led to the identification [42] of one of the 9-ring products, benzo[*cd*]phenanthro[1,2,3-*lm*]perylene, a $C_{34}H_{18}$ PAH that has never before been reported in the chemical literature.

Supercritical pyrolysis experiments with the model fuel toluene and HPLC/UV/MS analysis of the reaction products, in conjunction with Annellation Theory, have led to the identification [58,61,68] of six eight-ring benzenoid $C_{28}H_{14}$ PAH products that have never before been identified as products of toluene pyrolysis or combustion. Determining, by HPLC/UV/MS, which particular PAH are produced and which are not has contributed to the elucidation of radical reaction mechanisms [17] responsible for PAH formation and growth in the supercritical toluene pyrolysis environment. As in the case of 1-methylnaphthalene, there is no evidence of aromatic ring rupture in the supercritical toluene pyrolysis reaction environment, and PAH growth proceeds by combination of species plentiful in this environment—in this case, benzyl, phenyl, and methyl radicals, as well as toluene itself. These proposed reaction pathways [17] account for the formation of the six observed $C_{28}H_{14}$ PAH products and explain why the other two benzenoid

$C_{28}H_{14}$ PAH, determined by HPLC/UV/MS and Annellation Theory not to be present [58,68], are not formed. The detection, by HPLC/UV/MS, of seven 10-ring $C_{34}H_{16}$ and three 11-ring $C_{36}H_{16}$ PAH in the supercritical toluene pyrolysis products indicates that the benzyl-, phenyl-, and methyl-addition reactions responsible for the formation of the $C_{28}H_{14}$ PAH also take place with the $C_{28}H_{14}$ PAH products themselves, producing the higher-ring-number $C_{34}H_{16}$ and $C_{36}H_{16}$ products—and, by extension, carbonaceous solids.

Supercritical pyrolysis experiments with the model “endothermic” fuel methylcyclohexane yield toluene as the chief aromatic product. This fact—coupled with the finding, from HPLC/UV analyses of the reaction products, that the PAH product distribution from methylcyclohexane is almost the same as that from toluene—indicates that the reaction mechanisms [17] devised for PAH formation in the supercritical toluene pyrolysis environment are most likely to apply to the supercritical methylcyclohexane pyrolysis environment as well.

HPLC/UV/MS analyses of the supercritical pyrolysis products in a stressed Fischer-Tropsch synthetic jet fuel sample provided by UTRC (at the instigation of Dr. Tim Edwards at AFRL) have led to the identification of over 80 PAH of two to ten fused aromatic rings—many of which have never before been identified as products of alkane pyrolysis or combustion. Several of the identified PAH from the Fischer-Tropsch fuel do not appear in the products of our model aromatic fuels and have particularly high length-to-breadth ratios, a property that may be related to the long-chain alkane nature of the Fischer-Tropsch fuel. Because the UTRC tests have shown that this Fischer-Tropsch synthetic jet fuel is particularly prone to forming carbonaceous solids, supercritical pyrolysis experiments with representative alkanes are a major focus of our work on the AFOSR grant that has succeeded the one covered in the present report. It is anticipated that the model fuel experiments and HPLC/UV/MS analyses will play a major role in product

identification and reaction mechanism determination for the alkane fuels, just as they have already been shown to do in the cases of the model fuels examined so far.

Personnel who Performed the Research

Principal Investigator: Professor Mary Julia Wornat

Post-Doctoral Research Associates: Dr. Elmer B. Ledesma (November 1, 2003, to July 31, 2005); Dr. Jennifer W. McClaine (August 1, 2005, to September 30, 2006)

Graduate Students: Mr. Jorge O. Oña (supported by grant); Ms. Michelle L. Somers (supported by LSU Department of Chemical Engineering)

Publications and Presentations

Refereed publications reporting results from the research supported by this grant

Ledesma, E. B., Wornat, M. J., Felton, P. G., and Sivo, J. A., "The Effects of Pressure on the Yields of Polycyclic Aromatic Hydrocarbons Produced During the Supercritical Pyrolysis of Toluene," *Proceedings of the Combustion Institute* 30: 1371-1379 (2005).

McClaine, J. W., Zhang, X., and Wornat, M. J., "First Identification of Benzo[ghi]naphtho[8,1,2-bcd]perylene as a Product of Fuel Pyrolysis Using High-Performance Liquid Chromatography with Diode-Array Ultraviolet-Visible Absorbance Detection and Mass Spectrometry," *Journal of Chromatography A* 1127: 137-146 (2006).

Somers, M. L., McClaine, J. W., and Wornat, M. J., "The Formation of Polycyclic Aromatic Hydrocarbons from the Supercritical Pyrolysis of 1-Methylnaphthalene," *Proceedings of the Combustion Institute* 31: 501-509 (2007). [For this paper, the graduate student Michelle Somers won the James E. Peters Fellowship from the Central States Section of the Combustion Institute.]

McClaine, J. W., Oña, J. O., and Wornat, M. J., "Identification of a New C₂₈H₁₄ Polycyclic Aromatic Hydrocarbon as a Product of Supercritical Fuel Pyrolysis: Tribenzo[cd,ghi,lm]perylene," *Journal of Chromatography A* 1138: 175-183 (2007).

McClaine, J. W., and Wornat, M. J., "Reaction Mechanisms Governing the Formation of Polycyclic Aromatic Hydrocarbons in the Supercritical Pyrolysis of Toluene: C₂₈H₁₄ Isomers," *Journal of Physical Chemistry C* 111: 86-95 (2007).

Oña, J. O., and Wornat, M. J., "Identification of the C₃₀H₁₆ Polycyclic Aromatic Hydrocarbon Benzo[cd]naphtho[1,2,3-lm]perylene as a Product of Supercritical Pyrolysis of a Synthetic Jet Fuel," *Polycyclic Aromatic Compounds* 27, in press (2007).

Somers, M. L., and Wornat, M. J., "UV Spectral Identification of Polycyclic Aromatic Hydrocarbon Products of Supercritical 1-Methylnaphthalene Pyrolysis," accepted for publication in *Polycyclic Aromatic Compounds* (2007).

Oña, J. O., and Wornat, M. J., "The Influence of Solvents on the Ultraviolet-Visible Absorption Spectra of Polycyclic Hydrocarbons: Applications in the Identification of Fuel Products by HPLC/UV/MS," to be submitted to *Chromatographia*.

Conference presentations reporting results from the research supported by this grant

Ledesma, E. B., Wornat, M. J., Felton, P. G., and Sivo, J. A., "The Effects of Pressure on the Yields of Polycyclic Aromatic Hydrocarbons Produced During the Supercritical Pyrolysis of Toluene," accepted paper presented at the Thirtieth International Symposium on Combustion, Chicago, Illinois, July, 2004.

Oña, J. O., Ledesma, E. B., and Wornat, M. J., "Polycyclic Aromatic Hydrocarbons from the Supercritical Pyrolysis of Methylcyclohexane," work-in-progress poster presented at the Thirtieth International Symposium on Combustion, Chicago, Illinois, July, 2004.

Wornat, M. J., "PAH Formation Mechanisms for Aromatic Components of Solid and Liquid Fuels," invited talk at the Two-Hundred Twenty-Eighth National Meeting of the American Chemical Society, Philadelphia, Pennsylvania, August, 2004.

Somers, M. L., and Wornat, M. J., "PAH Production from the Supercritical Pyrolysis of 1-Methylnaphthalene" Twentieth International Symposium on Polycyclic Aromatic Compounds, Toronto, Canada, August, 2005.

Oña, J. O., and Wornat, M. J., "Ring-Closure Scheme for the Formation of Large Polycyclic Aromatic Hydrocarbons from the Supercritical Pyrolysis of Methylcyclohexane," Twentieth International Symposium on Polycyclic Aromatic Compounds, Toronto, Canada, August, 2005. [Graduate student Jorge Oña won the Erich Clar Award for the best paper presented orally by a student at this conference.]

Zhang, X., Somers, M. L., Robles, J. A., and Wornat, M. J., "Detection of Polycyclic Aromatic Hydrocarbons by Liquid Chromatography / Atmospheric-Pressure Photoionization Mass Spectrometry," poster presentation at the Fifty-Fourth ASMS Conference on Mass Spectrometry and Allied Topics, Seattle, Washington, May, 2006.

Somers, M. L., McClaine, J. W., and Wornat, M. J., "The Formation of Polycyclic Aromatic Hydrocarbons from the Supercritical Pyrolysis of 1-Methylnaphthalene," accepted paper presented at the Thirty-First International Symposium on Combustion, Heidelberg, Germany, August, 2006.

Oña, J. O., and Wornat, M. J., "Perylene Benzologues: A Major Class of PAH Products from the Supercritical Pyrolysis of a Synthetic Jet Fuel," work-in-progress poster presented at the Thirty-First International Symposium on Combustion, Heidelberg, Germany, August, 2006.

McClaine, J. W., Zhang, X., Oña, J. O., and Wornat, M. J., "Identification of Benzo[ghi]naphtho[8,1,2-bcd]perylene: a New 8-Ring Benzenoid PAH Found as a Product of Supercritical Toluene Pyrolysis," work-in-progress poster presented at the Thirty-First International Symposium on Combustion, Heidelberg, Germany, August, 2006.

Somers, M. L., Zhang, X., and Wornat, M. J., "The Detection and Identification of Polycyclic Aromatic Hydrocarbon Products from 1-Methylnaphthalene Pyrolysis," work-in-progress poster presented at the Thirty-First International Symposium on Combustion, Heidelberg, Germany, August, 2006.

Bagley, S. P., Oña, J. O., and Wornat, M. J., "Formation of Polycyclic Aromatic Hydrocarbons from a Fischer-Tropsch Jet Fuel," work-in-progress poster presented at the Thirty-First International Symposium on Combustion, Heidelberg, Germany, August, 2006.

Oña, J. O., and Wornat, M. J., "Identification of PAH with More than Eight Rings from a Sample of the Supercritical Pyrolysis of Fischer-Tropsch Synthetic Jet Fuel," Southeastern Regional Meeting of the American Chemical Society, Augusta, Georgia, November, 2006.

Edwards, J. T., DeWitt, M. J., Shafer, L., Brooks, D., Huang, H., Bagley, S. P., Oña, J. O., and Wornat, M. J., "Fuel Composition Influence on Deposition in Endothermic Fuels," paper AIAA-2006-7973, Fourteenth International Space Planes and Hypersonics Systems and Technologies Conference, Canberra, Australia, November, 2006.

References

1. T. Edwards, S. Zabarnick, *Industrial and Engineering Chemistry Research* 32 (1993) 3117-3122.
2. S. P. Heneghan, S. Zabarnick, D. R. Ballal, W. E. Harrison III, *Journal of Energy Resources Technology* 118 (1996) 170-179.
3. T. Doungthip, J. S. Ervin, T. F. Williams, J. Bento, *Industrial and Engineering Chemistry Research* 41 (2002) 5856-5866.
4. T. Edwards, *Combustion Science and Technology* 178 (2006) 307-334.
5. T. Edwards, personal communication, AFRL, Wright-Patterson, Ohio, June 12, 2002.
6. C. F. Melius, N. E. Bergan, J. E. Shepherd, *Proceedings of the Combustion Institute* 23 (1990) 217-223.
7. K. P. Johnston, C. Haynes, *AIChE Journal* 33 (1987) 2017-2026.
8. M. E. Paulaitis, G. C. Alexander, *Pure and Applied Chemistry* 59 (1987) 61-68.
9. R. H. Helling, J. W. Tester, *Energy & Fuels* 1 (1987) 417-423.
10. C. A. Eckert, B. E. Knutson, P. G. Debenedetti, *Nature* 383 (1996) 313-318.
11. J. F. Stewart, *Supercritical Pyrolysis of Endothermic Fuels*. Ph.D. Thesis, Department of Mechanical and Aerospace Engineering, Princeton University, 1999.

12. J. F. Stewart, K. Brezinsky, I. Glassman, *Combustion Science and Technology* 136 (1998) 373-390.
13. H. Bockhorn, F. Fetting, H. W. Wenz, *Berichte der Bunsen-Gesellschaft—Physical Chemistry Chemical Physics* 87 (1983) 1067-1073.
14. M. Frenklach, D. W. Clary, W. C. J. Gardiner, S. E. Stein, *Proceedings of the Combustion Institute* 20 (1984) 887-901.
15. H. Wang, M. Frenklach, *Combustion and Flame* 110 (1997) 173-221.
16. E. B. Ledesma, M. J. Wornat, P. G. Felton, J. A. Sivo, *Proceedings of the Combustion Institute* 30 (2005) 1371-1379.
17. J. W. McClaine, M. J. Wornat, *Journal of Physical Chemistry C* 111 (2007) 86-95.
18. M. Bernabei, R. Reda, R. Galiero, G. Bocchinfuso, *Journal of Chromatography A* 985 (2003) 197-203.
19. G. D. Davis, *An Experimental Study of Supercritical Methylcyclohexane Pyrolysis*. M.S.E. Thesis, Department of Mechanical and Aerospace Engineering, Princeton University, 1994.
20. M. L. Somers, J. W. McClaine, M. J. Wornat, *Proceedings of the Combustion Institute* 31 (2007) 501-509.
21. S. Darrah, "Jet Fuel Deoxygenation," AFWAL-TR-88-2081 (1988).
22. A. H. Cutler, M. J. Antal, M. Jones, *Industrial and Engineering Chemistry Research* 27 (1988) 691-697.
23. J. C. Y. Lee, *Simulations of Two-Dimensional Chemically Reactive Flows: Flow Past a Fuel Particle and Inside a Reactor Tube*. Ph.D. Thesis, Department of Mechanical and Aerospace Engineering, Princeton University, 1996.
24. R. N. Jones, *Journal of the American Chemical Society* 67 (1945) 2127-2150.
25. J. C. Fetzer, *Large ($C \geq 24$) Polycyclic Aromatic Hydrocarbons: Chemistry and Analysis*. Wiley-Interscience, New York, 2000.
26. E. V. Dose, G. Guiochon, *Analytical Chemistry* 61 (1989) 2571-2579.
27. S. J. Bos, S. M. van Leeuwen, U. Karst, *Analytical and Bioanalytical Chemistry* 384 (2006) 85-99.
28. H. Huang, D. R. Sobel, L. J. Spadaccini, Paper AIAA 2002-3871 of the 38th AIAA/ASME/SAE/ASEE Joint Propulsion Conference and Exhibit, Indianapolis, Indiana, July, 2002.

29. M. L. Somers, M. J. Wornat, accepted for publication in *Polycyclic Aromatic Compounds*.
30. E. D. Bergmann, E. Fischer, Y. Hirshberg, D. Lavie, Y. Sprinzak, J. Szmuszkowicz, *Mémoires Présentés à la Société Chimique* 1953 (1953) 798-809.
31. L. Xiujin, *Scientia Sinica (Series B)* 29 (1986) 481-493.
32. S. P. Bagley and M. J. Wornat, accepted for presentation at the Twenty-First International Symposium on Polycyclic Aromatic Compounds, to be held in Trondheim, Norway, August, 2007.
33. S. A. Wise, R. M. Campbell, W. R. West, M. L. Lee, K. D. Bartle, *Chemical Geology* 54 (1986) 339-357.
34. K. F. Lang, H. Buffleb, *Chemische Berichte* 91 (1958) 2866-2870.
35. J. Yang, M. Lu, *Environmental Science and Technology* 39 (2005) 3077-3082.
36. W. Lijinsky, C. R. Raha, *Journal of Organic Chemistry* 26 (1961) 3566-3568.
37. W. Schmidt, G. Grimmer, J. Jacob, G. Dettbarn, K. W. Naujack, *Fresenius' Zeitschrift für Analytische Chemie* 326 (1987) 401-413.
38. L. C. Sander, S. A. Wise, *NIST Special Publication 922 "Polycyclic Aromatic Hydrocarbon Structure Index,"* <http://ois.nist.gov/pah/search.cfm> (1997).
39. Y.-R. Luo, *Handbook of Bond Dissociation Energies in Organic Chemistry*. CRC Press, Boca Raton, FL, 2003, pp. 38, 39, 110.
40. R. T. Sanderson, *Chemical Bonds in Organic Compounds*. Sea and Sand, Scottsdale, AZ, 1976, Chapter 8.
41. M. Szwarc, A. Shaw, *Journal of the American Chemical Society* 73 (1951) 1379.
42. M. L. Somers, M. J. Wornat, in preparation.
43. J. V. Knop, W. R. Mueller, K. Szymanskik, N. Trinajstic, *Computer Generation of Certain Classes of Molecules*. SKTH/Kemija u Industriji, Zegreb, 1985, 210 pages.
44. M. Zander, W. Franke, *Chemische Berichte* 94 (1961) 446-450.
45. E. J. Clar, *Journal of the Chemical Society [Abstracts]* 1949 (1949) 2013-2016.
46. K. F. Lang, M. Zander, *Chemische Berichte* 98 (1965) 597-600.
47. E. J. Clar, B. A. McAndrew, J. F. Stephen, *Tetrahedron* 26 (1970) 5465-5478.
48. K. Maruyama, T. Otsuki, K. Mitsui, *Journal of Organic Chemistry* 45 (1980) 1424-1428.

49. E. J. Clar, *Polycyclic Hydrocarbons*, Volume 2. Academic Press, New York, 1964.
50. J. C. Fetzer, Chapter 18 in *Polynuclear Aromatic Hydrocarbons*, ed. by L. Ebert. *Advances in Chemistry* 217. American Chemical Society, Washington, D. C., 1988, pp. 309-331.
51. J. C. Fetzer, W. R. Biggs, *Journal of Chromatography* 322 (1985) 275-286.
52. J. C. Fetzer, W. Schmidt, *Spectrochimica Acta A* 45A (1989) 503-505.
53. E. J. Clar, J. F. Guye-Vuilleme, J. F. Stephen, *Tetrahedron* 20 (1964) 2107-2117.
54. S. A. Wise, L. C. Sander, W. E. May, *Journal of Chromatography* 642 (1993) 329-349.
55. L. C. Sander, M. Pursch, S. A. Wise, *Analytical Chemistry* 71 (1999) 4821-4830.
56. S. A. Wise, L. C. Sander, *Journal of High Resolution Chromatography & Chromatography Communications* 8 (1985) 248-255.
57. T. Umemoto, T. Kawashima, Y. Sakata, S. Misumi, *Tetrahedron Letters* 12 (1975) 1005-1006.
58. J. W. McClaine, X. Zhang, M. J. Wornat, *Journal of Chromatography A* 1127 (2006) 137-146.
59. E. J. Clar, *The Aromatic Sextet*. Wiley-Interscience, New York, 1972.
60. M. J. Wornat, Final Performance Report for AFOSR DURIP Grant No. FA9550-05-1-0253 (2006).
61. M. J. Wornat, E. B. Ledesma, J. W. McClaine, J. O. Oña, in preparation.
62. J. C. Fetzer, W. R. Biggs, K. Jinno, *Chromatographia* 21 (1986) 439-442.
63. J. C. Fetzer, J. R. Kershaw, *Fuel* 74 (1995) 1533-1536.
64. A. L. Lafleur, K. Taghizadeh, J. B. Howard, J. F. Anacleto, M. A. Quilliam *Journal of the American Society of Mass Spectrometry* 7 (1996) 276-286.
65. J. C. Fetzer, W. R. Biggs, *Polycyclic Aromatic Compounds* 5 (1994) 193-198
66. L. Ojakaar, *The Synthesis of Some New Aromatic Polycyclic Hydrocarbons*. Ph.D. Thesis, Department of Chemistry, Virginia Polytechnic University, 1964.
67. F. A. Vingiello, L. Ojakaar, *Tetrahedron* 22 (1966) 847-860.
68. J. W. McClaine, J. O. Oña, M. J. Wornat, *Journal of Chromatography A* 1138 (2007) 175-183.

69. M. Zander, W. Franke, *Chemische Berichte* 99 (1966) 1275-1278.
70. A. L. Lafleur, P. A. Monchamp, E. F. Plummer, M. J. Wornat, *Analytical Letters* 20 (1987) 1171-1192.
71. M. J. Wornat, Final Technical Report for AFOSR Grant No. F49620-00-1-0298 (2003).
72. T. Edwards, personal communication, AFRL, Wright-Patterson, Ohio, October, 2005.
73. J. O. Oña, M. J. Wornat, *Polycyclic Aromatic Compounds* 27 (2007) in press.
74. J. O. Oña, M. J. Wornat, to be submitted to *Chromatographia*.

Table 1 (continued). Products of Supercritical 1-Methylnaphthalene Pyrolysis at 585°C, 110 atm, 140 sec. Results from Somers, McClaine, and Wornat [20].

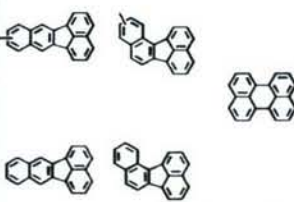
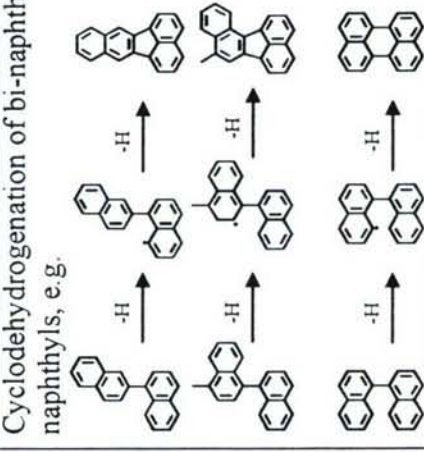
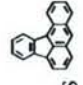

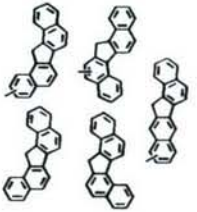
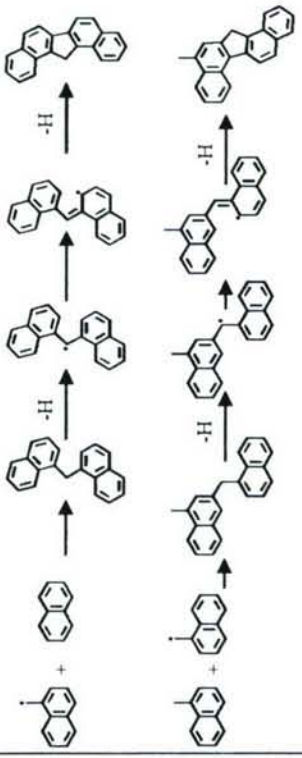
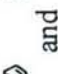
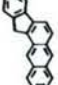
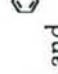
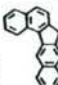
Products	Reactions Responsible for Product Formation	Findings
	<p>Cyclodehydrogenation of bi-naphthyls and methylated bi-naphthyls, e.g.</p> 	<p>The intactness of the original two 2-ring naphthalene units is preserved in the C₂₀H₁₂ five-ring PAH products.</p> <p>Isomers of the Class 3 products such as  and  are not produced since their formation does not require the addition of two 2-ring naphthalene units but rather a 1-ring and a 3-ring structure, which are not present in the supercritical 1-methylnaphthalene pyrolysis environment.</p>
	<p>1-naphthylmethyl radical displacement of an aryl H of either naphthalene or a methylnaphthalene, followed by dehydrogenation, e.g.</p> 	<p>The intactness of the original two 2-ring naphthalene units is preserved in the C₂₁H₁₄ five-ring PAH products.</p> <p>Isomers of the Class 4 products such as  and  are not produced since their formation does not require the addition of two 2-ring naphthalene units but rather a 1-ring and a 3-ring structure, which are not present in the supercritical 1-methylnaphthalene pyrolysis environment.</p> <p>Isomers of the Class 4 products such as  and  are not observed here either since their formation requires a 2-naphthylmethyl adding to a "2" position of naphthalene, rather than the more plentiful 1-naphthylmethyl and "1" position.</p>

Table 1 (continued). Products of Supercritical 1-Methylnaphthalene Pyrolysis at 585°C, 110 atm, 140 sec. Results from Somers, McClaine, and Wornat [20].

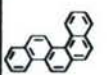

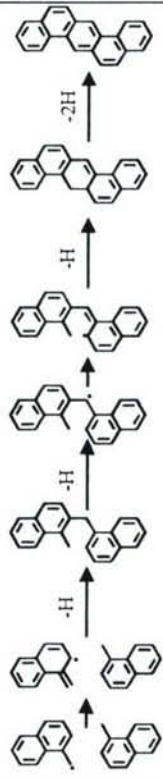
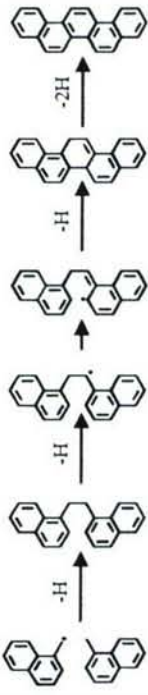
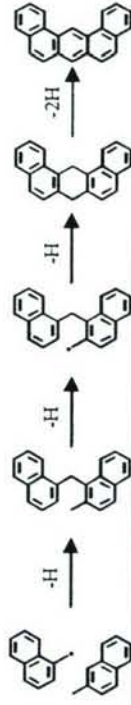

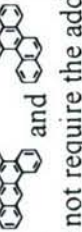

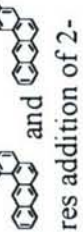
Products	Reactions Responsible for Product Formation	Findings
 	<p>Class 5: Five-Ring C₂₂H₁₄ PAH (red structures in Figure 2)</p> <p>Addition of 1-naphthylmethyl radical (or its resonance structure) to either 1-methylnaphthalene or 2-methylnaphthalene, followed by dehydrogenation, e.g.</p>   	<p>The intactness of the original two 2-ring naphthalene units is preserved in the C₂₂H₁₄ five-ring PAH products.</p> <p>Isomers of the Class 5 products such as  and  are not produced since their formation does not require the addition of two 2-ring naphthalene units but rather one 2-ring naphthalene unit and two 1-ring structures, the latter of which are not present in the supercritical 1-methylnaphthalene pyrolysis environment.</p> <p>Isomers of the Class 5 products such as  and  are not observed since their formation requires addition of 2-naphthylmethyl radical to 2-methylnaphthalene, which are much less plentiful than the "1-" counterparts in a 1-methylnaphthalene reaction environment.</p>

Table 1 (continued). Products of Supercritical 1-Methylnaphthalene Pyrolysis at 585°C, 110 atm, 140 sec. Results from Somers, McClaine, and Wornat [20].


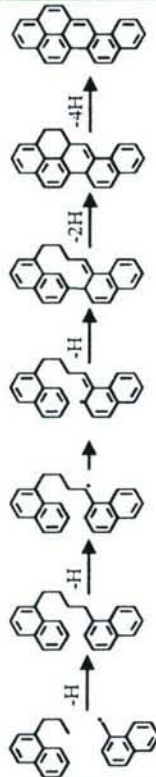
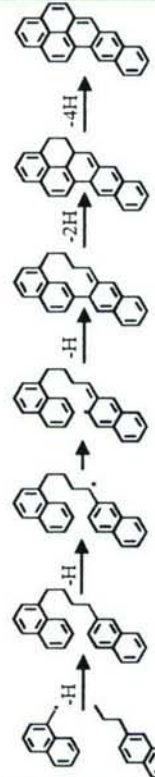

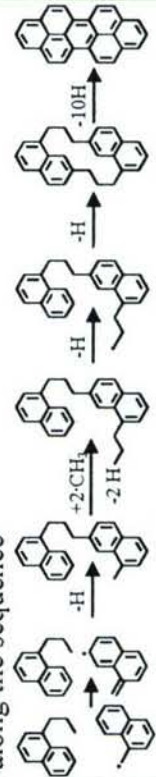




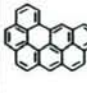


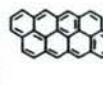
Products	Reactions Responsible for Product Formation	Findings
Class 6: Six- and Seven-Ring PAH		
(a) C ₂₄ H ₁₄ PAH and CH ₃ -C ₂₄ H ₁₃ PAH	(a) Methyl addition twice to a methylnaphthalene to form a propylnaphthalene, then addition of 1-naphthylmethyl and dehydrogenation	(a) C ₂₄ H ₁₄ isomers such as  (i) (ii) (iii) and (iv) are not formed since: (i) their structures do not preserve the intactness of two 2-ring naphthalene units, (ii) their formation would require at least one of the naphthalene units to have been alkylated in the "2" position, (iii) their formation would require the methyl additions to occur at aryl rather than alkyl positions (the latter being favored for BDE reasons), or (iv) their formation would require the reaction of 1-naphthylethyl with 1-ethylnaphthalene, an unlikely scenario in a reaction environment dominated by 1-methylnaphthalene.
Naphtho[2,1- <i>a</i>]pyrene		
Naphtho[2,3- <i>a</i>]pyrene		
Methylated naphtho[2,1- <i>a</i>]pyrene		
(b) C ₂₆ H ₁₄	(b) Same as (a) but with two additional methyl additions along the sequence	(b) Just as in the cases of the 5- and 6-ring products, high product selectivity is observed for the 7-ring PAH, as dibenzo[<i>cd,m</i>]perylene is the only C ₂₆ H ₁₄ product detected.
Dibenzo[<i>cd,m</i>]perylene		

Table 2. The Eight Theoretically Possible Benzenoid $C_{28}H_{14}$ PAH

Benzo[<i>a</i>]coronene		Established [61] as products of supercritical toluene pyrolysis by matching UV spectra with those of authentic reference standards
Benzo[<i>pqr</i>]naphtho[8,1,2- <i>bcd</i>]perylene		
Phenanthro[5,4,3,2- <i>efghi</i>]perylene		Established [61] as products of supercritical toluene pyrolysis by confirming $C_{28}H_{14}$ formulas from mass spectra and matching UV spectra with those published for the reference standards
Benzo[<i>cd</i>]naphtho[8,1,2,3- <i>fghi</i>]perylene		
Benzo[<i>ghi</i>]naphtho[8,1,2- <i>bcd</i>]perylene		Deduced [58,68] as products of supercritical toluene pyrolysis from HPLC elution times, mass spectra, UV spectra, and Annellation Theory
Tribenzo[<i>cd,ghi,lm</i>]perylene		
Bisanthene		Determined [58,68] not to be a product of supercritical toluene pyrolysis, from the published UV spectrum of the reference standard [49]
Naphthaceno[3,4,5,6,7- <i>defghij</i>]naphthacene		Deduced [58,68] not to be a product of supercritical toluene pyrolysis, from UV spectral characteristics predicted from Annellation Theory

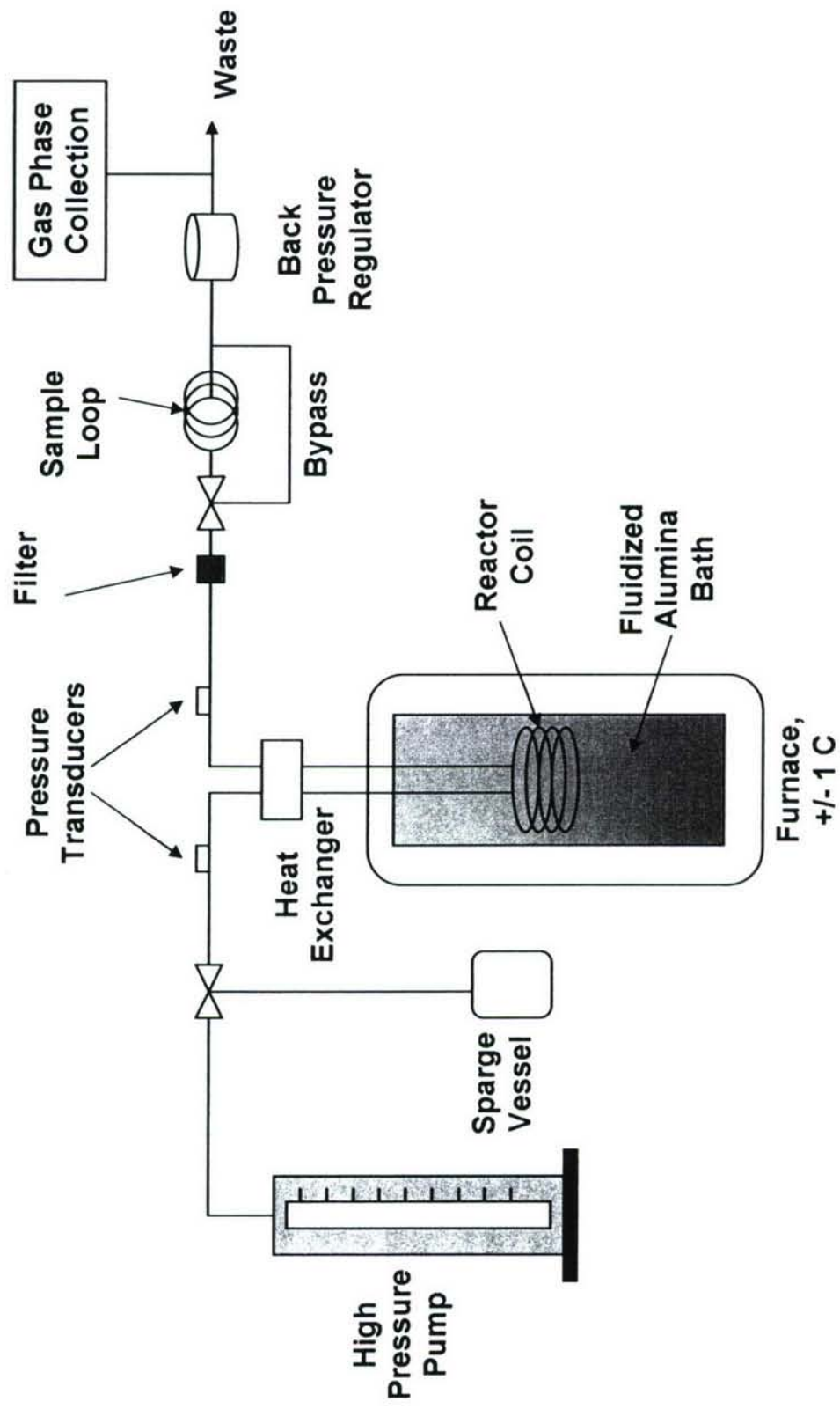


Figure 1. Supercritical fuels pyrolysis reactor system. Adapted from Stewart [11].

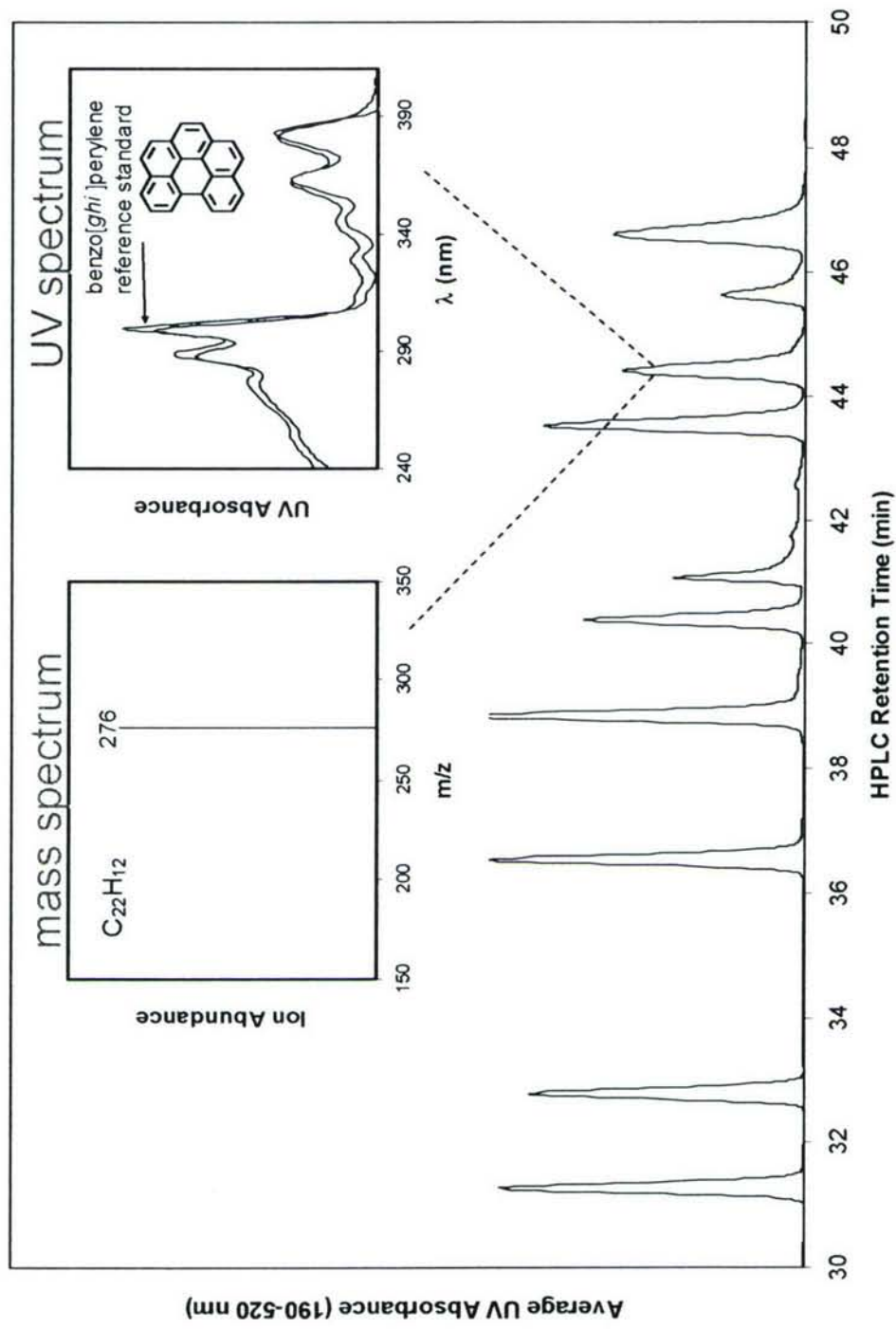


Figure 2. Illustration of the HPLC/UV/MS analysis technique. The left inset is the mass spectrum of the component eluting at 44.4 min in the HPLC chromatogram. The black curve in the right inset is the UV spectrum of this same component; the red curve in the right inset is the UV spectrum of a reference standard of benzo[ghi]perylene.

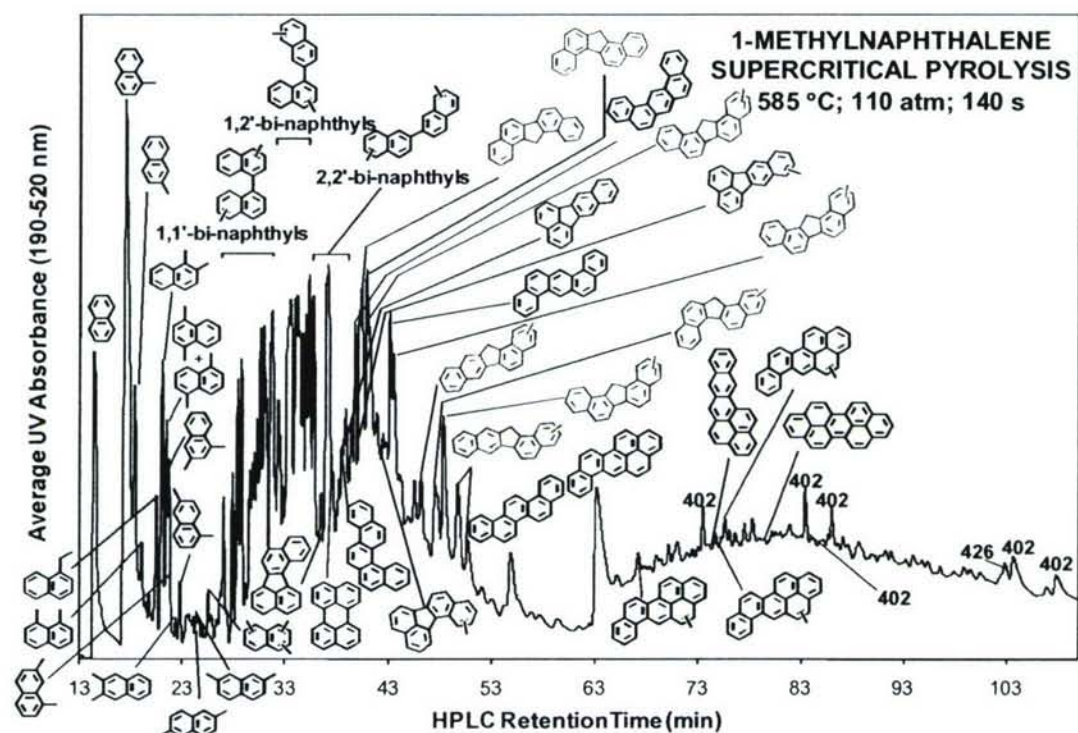


Figure 3. HPLC chromatogram of products of 1-methylnaphthalene pyrolyzed at 585 °C, 110 atm, and 140 sec. The rise in baseline at 63 minutes corresponds to a change in mobile-phase composition to UV-absorbing dichloromethane. Identified products of Classes 1 and 2 (in order of elution) are: naphthalene; 1-methylnaphthalene; 2-methylnaphthalene; 1,8-dimethylnaphthalene; 1-ethylnaphthalene; 1,2-dimethylnaphthalene; 1,4- and 1,5-dimethylnaphthalene; 1,3- and 1,7-dimethylnaphthalene; 2,3-dimethylnaphthalene; 1,6-dimethylnaphthalene; 2,6-dimethylnaphthalene; 2,7-dimethylnaphthalene; trimethylnaphthalene; 1,1'-bi-naphthyls; 1,2'-bi-naphthyls; and 2,2'-bi-naphthyls. Identified products of ≥ 5 rings, by class (in order of elution, from left to right) are: Class 3 (blue): benzo[*j*]fluoranthene; perylene; benzo[*k*]fluoranthene; methylbenzo[*k*]fluoranthene; methylbenzo[*j*]fluoranthene. Class 4 (green): dibenzo[*a,i*]fluorene; dibenzo[*a,g*]fluorene; methyldibenzo[*a,i*]fluorene; methyldibenzo[*a,i*]fluorene; methyldibenzo[*a,h*]fluorene; methyldibenzo[*a,g*]fluorene; methyldibenzo[*a,i*]fluorene; methyldibenzo[*a,h*]fluorene; methyldibenzo[*a,h*]fluorene. Class 5 (red): benzo[*c*]chrysene; dibenz[*a,j*]anthracene; dibenz[*a,h*]anthracene; picene. Class 6 (black): naphtho[2,1-*a*]pyrene; methylnaphtho[2,1-*a*]pyrene; naphtho[2,3-*a*]pyrene; methylnaphtho[2,1-*a*]pyrene; methylnaphtho[2,1-*a*]pyrene; dibenzo[*cd,lm*]perylene. Numbers “402” and “426” signify molecular masses of PAH whose exact structures have not yet been determined. Results from Somers, McClaine, and Wornat [20].

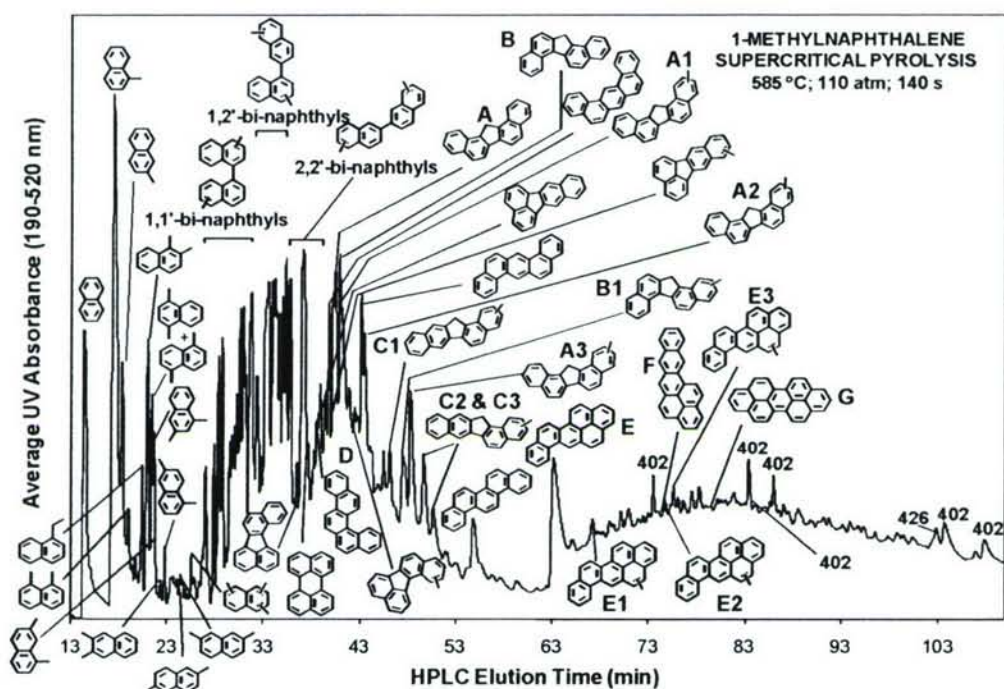


Figure 4. HPLC chromatogram of the products of 1-methylnaphthalene supercritical pyrolysis at 585°C, 110 atm, and 140 sec. Newly identified unsubstituted products are labelled with single letters **A-G**. Newly identified methyl-substituted PAH are labelled with a letter and a number—the letter designating the PAH base structure. Labels “402” and “426” designate molecular masses of product components that are not yet identified. The rise in baseline at ~63 minutes corresponds to a change in mobile phase composition to UV-absorbing dichloromethane. Results from Somers and Wornat [29].

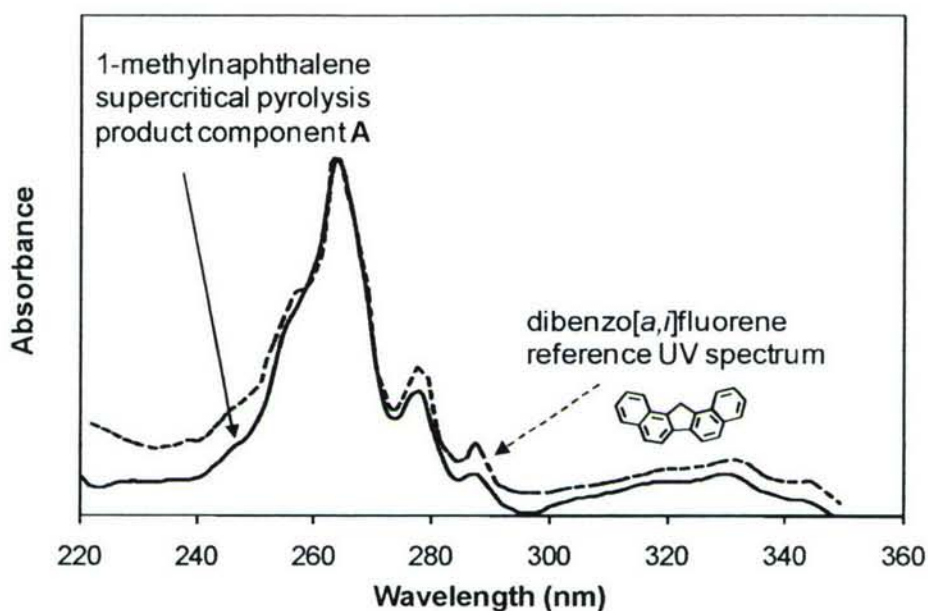


Figure 5. UV absorbance spectra of the reference standard [30,31] of dibenzo[*a,i*]fluorene (dashed) and of 1-methylnaphthalene pyrolysis product component **A** (solid). Results from Somers and Wornat [29].

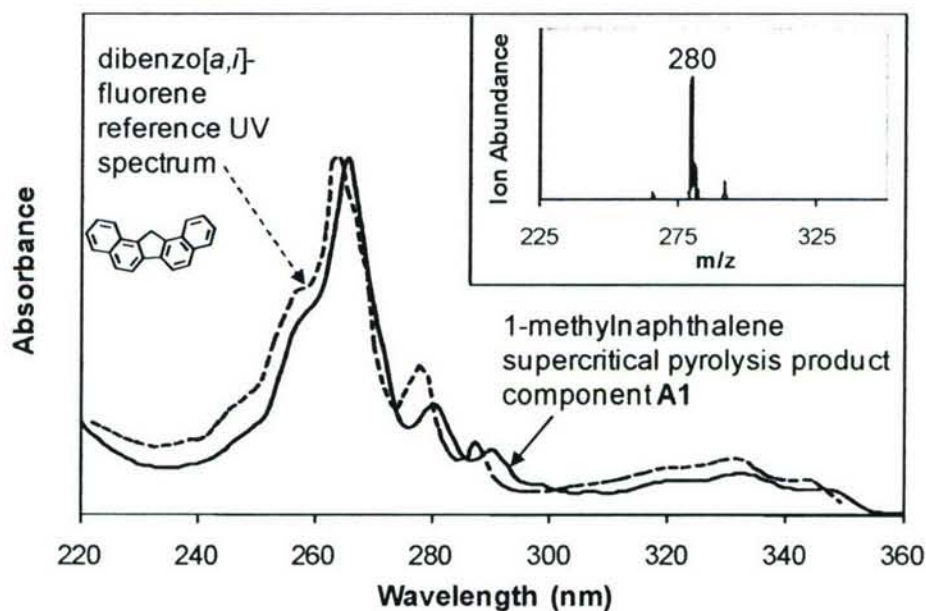


Figure 6. UV absorbance spectra of the reference standard [30,31] of dibenzo[*a,i*]fluorene (dashed) and of 1-methylnaphthalene pyrolysis product component **A1** (solid) along with the mass spectrum (inset) of component **A1**. The bathochromic shift in the UV spectrum of the product component indicates alkyl substitution; the mass spectrum indicates that the alkyl substituent is methyl. Results from Somers and Wornat [29].

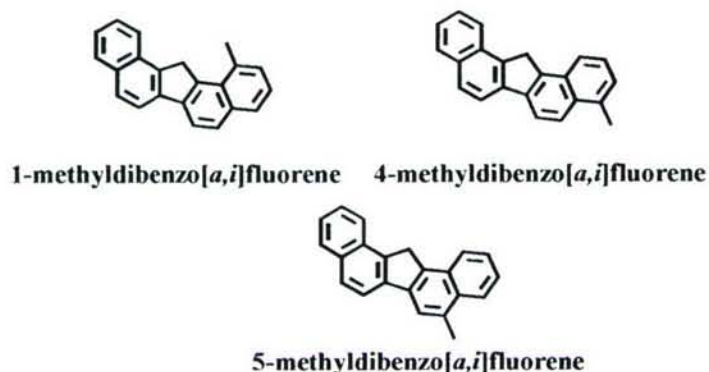


Figure 7. 1-methyldibenzo[*a,i*]fluorene, 4-methyldibenzo[*a,i*]fluorene, and 5-methyldibenzo[*a,i*]fluorene. These three isomers illustrate the three most likely positions of the methyl substituent for the three methyldibenzo[*a,i*]fluorene products (components **A1**, **A2**, and **A3**) according to the reaction schemes [20] involving combination of two 1-methylnaphthalene units. Results from Somers and Wornat [29].

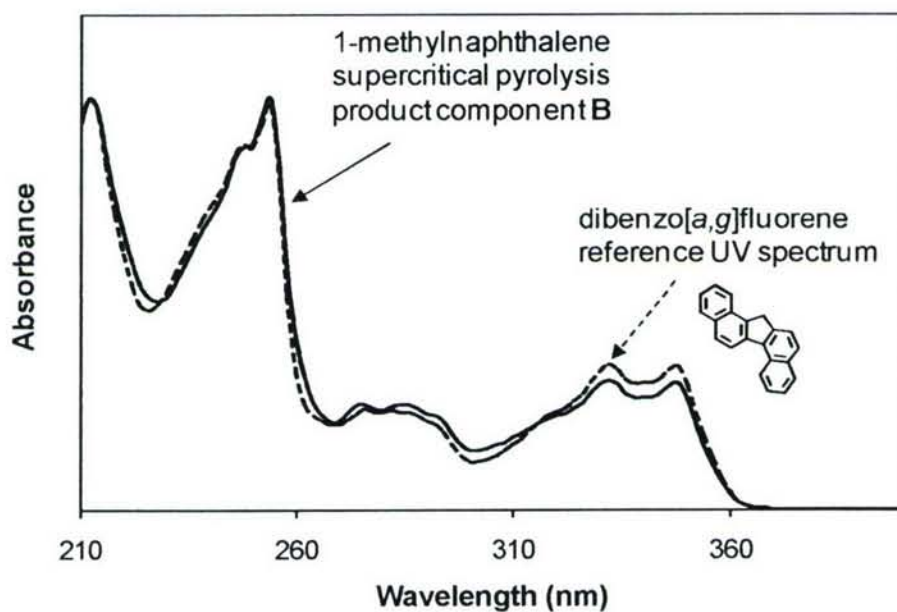


Figure 8. UV absorbance spectra of the reference standard of dibenzo[*a,g*]fluorene (dashed) and of 1-methylnaphthalene pyrolysis product component **B** (solid). Results from Somers and Wornat [29].

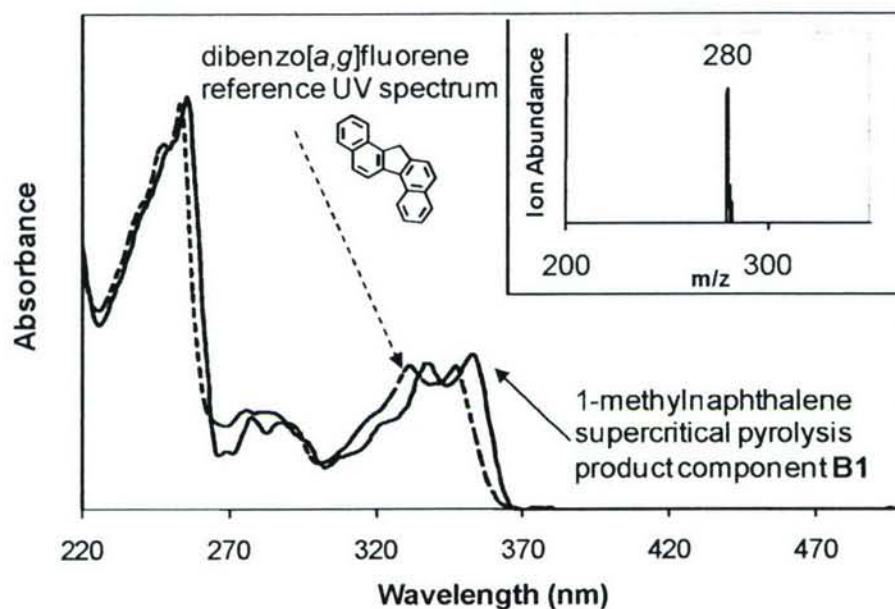


Figure 9. UV absorbance spectra of the reference standard of dibenzo[a,g]fluorene (dashed) and of 1-methylnaphthalene pyrolysis product component **B1** (solid) along with its mass spectrum (inset). The bathochromic shift in the UV spectrum of the product component indicates alkyl substitution; the mass spectrum indicates that the alkyl substituent is methyl. Results from Somers and Wornat [29].

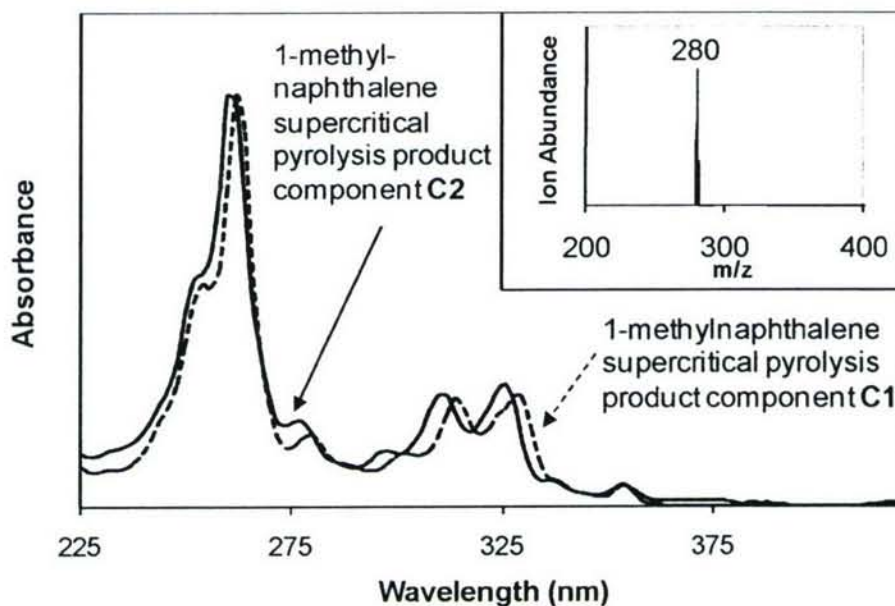


Figure 10. UV absorbance spectra of 1-methylnaphthalene pyrolysis product component **C1** (dashed) and of the 1-methylnaphthalene pyrolysis product component **C2** (solid), along with its mass spectrum (inset). Results from Somers and Wornat [29].

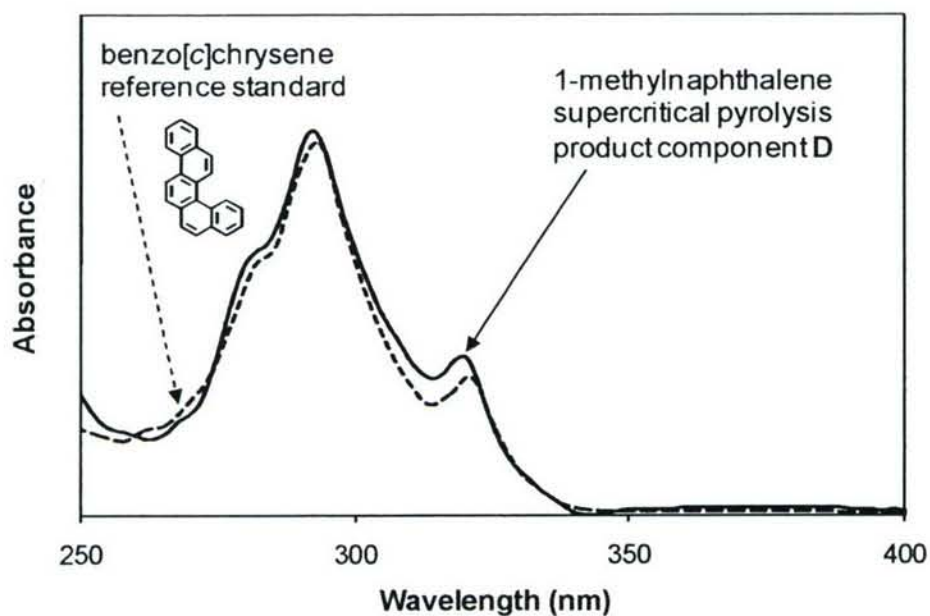


Figure 11. UV absorbance spectra of the reference standard of benzo[c]chrysene (dashed) and of 1-methylnaphthalene pyrolysis product component **D** (solid). Results from Somers and Wornat [29].

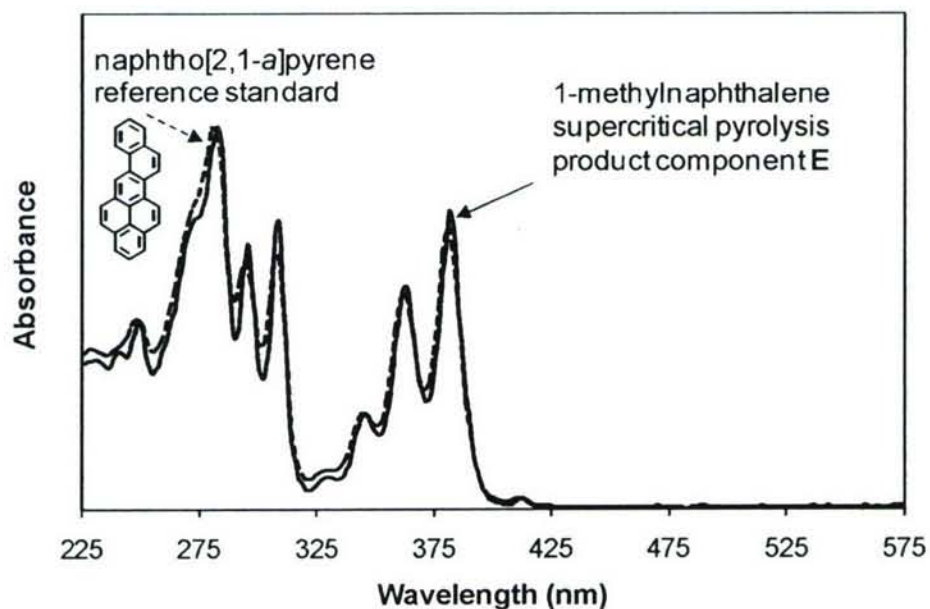


Figure 12. UV absorbance spectra of the reference standard of naphtho[2,1-a]pyrene (dashed) and of 1-methylnaphthalene pyrolysis product component **E** (solid). Results from Somers and Wornat [29].

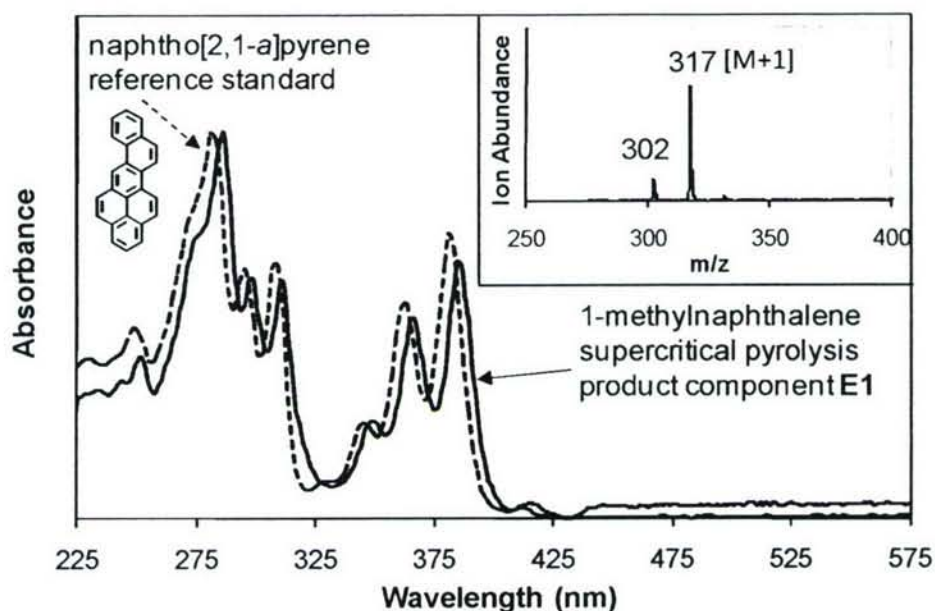


Figure 13. UV absorbance spectra of the reference standard of naphtho[2,1-a]pyrene (dashed) and of 1-methylnaphthalene pyrolysis product component **E1** (solid) along with its mass spectrum (inset). The bathochromic shift in the UV spectrum of the product component indicates alkyl substitution; the mass spectrum, with primary ion at M+1, indicates that the alkyl substituent is methyl. Results from Somers and Wornat [29].

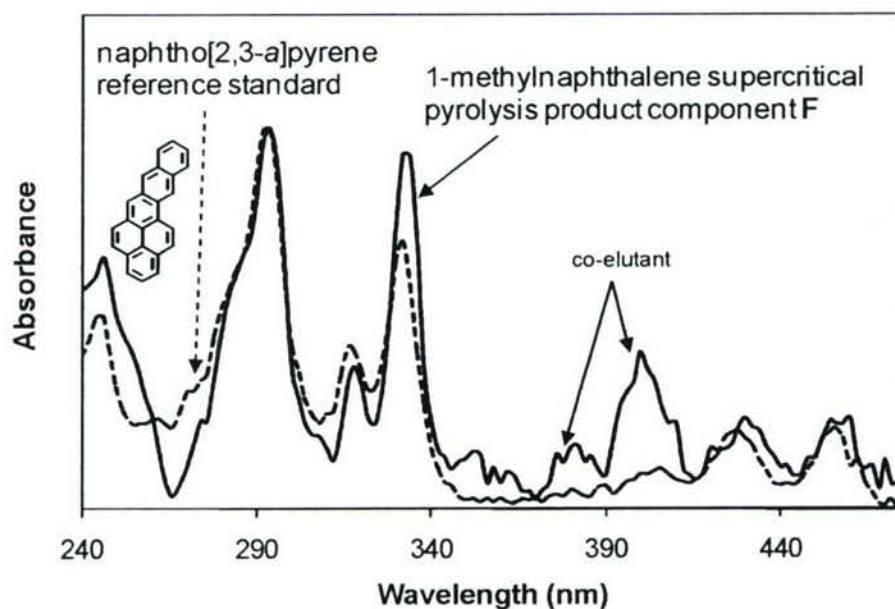


Figure 14. UV absorbance spectra of the reference standard of naphtho[2,3-a]pyrene (dashed) and of 1-methylnaphthalene pyrolysis product component **F** (solid). The peaks at 380 nm and 400 nm are from an unidentified co-eluting compound. Results from Somers and Wornat [29].

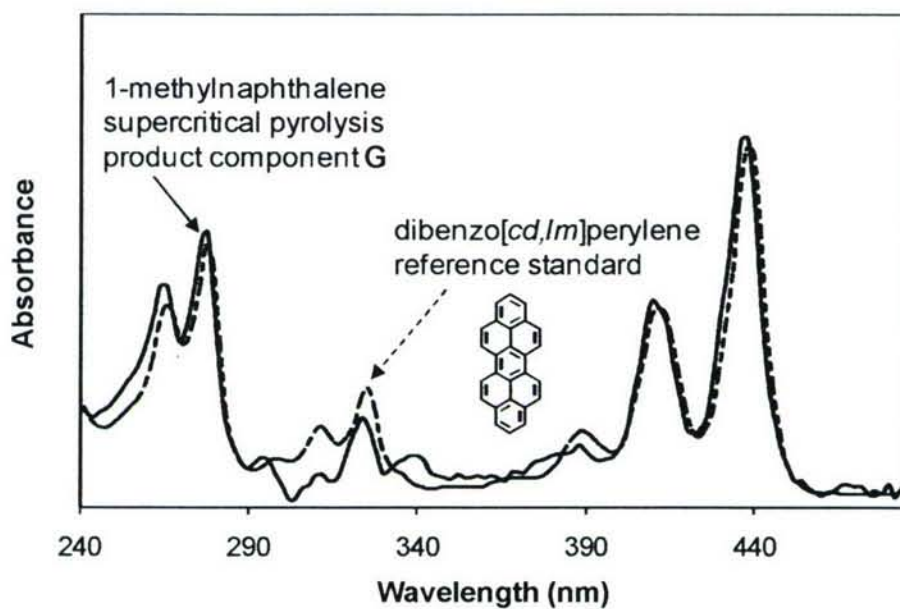


Figure 15. UV absorbance spectra of the reference standard of dibenzo[*cd,lm*]perylene (dashed) and of 1-methylnaphthalene pyrolysis product component **G** (solid). Results from Somers and Wornat [29].

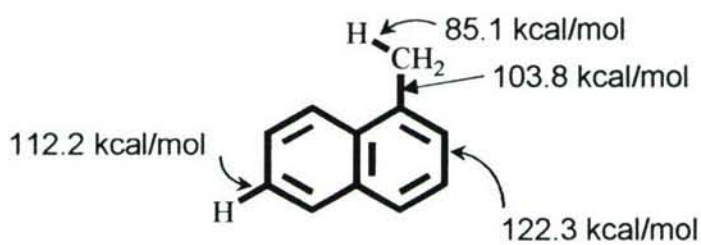


Figure 16. 1-Methylnaphthalene bond dissociation energies [39,40]

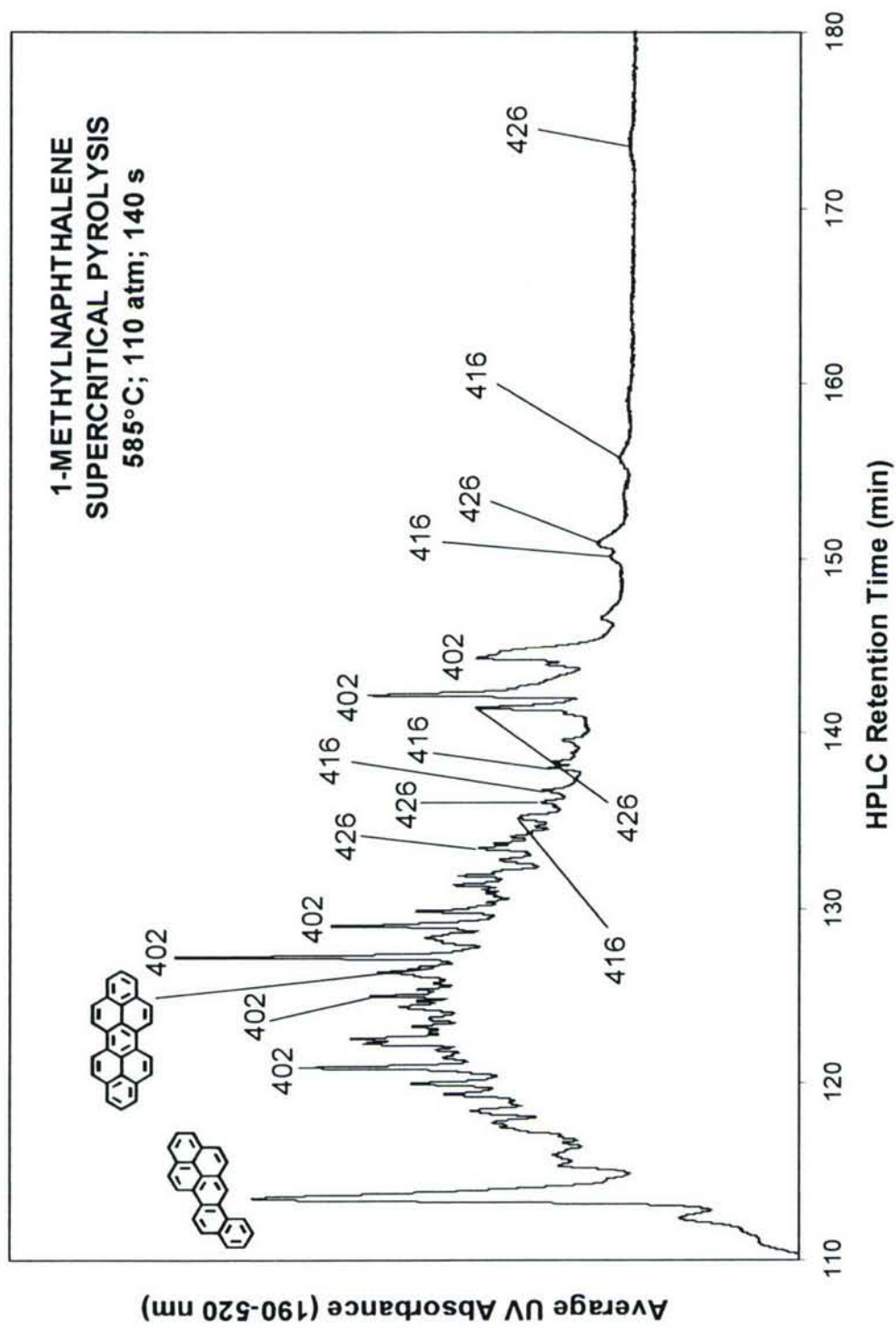


Figure 17. Final portion of the HPLC chromatogram (from a methanol/dichloromethane solvent program) of the products of 1-methylnaphthalene pyrolyzed at 585°C, 110 atm, and 140 sec. Numbers “402,” “416,” and “426” signify molecular masses of 8- and 9-ring PAH product components. Results from Somers and Wornat [42].

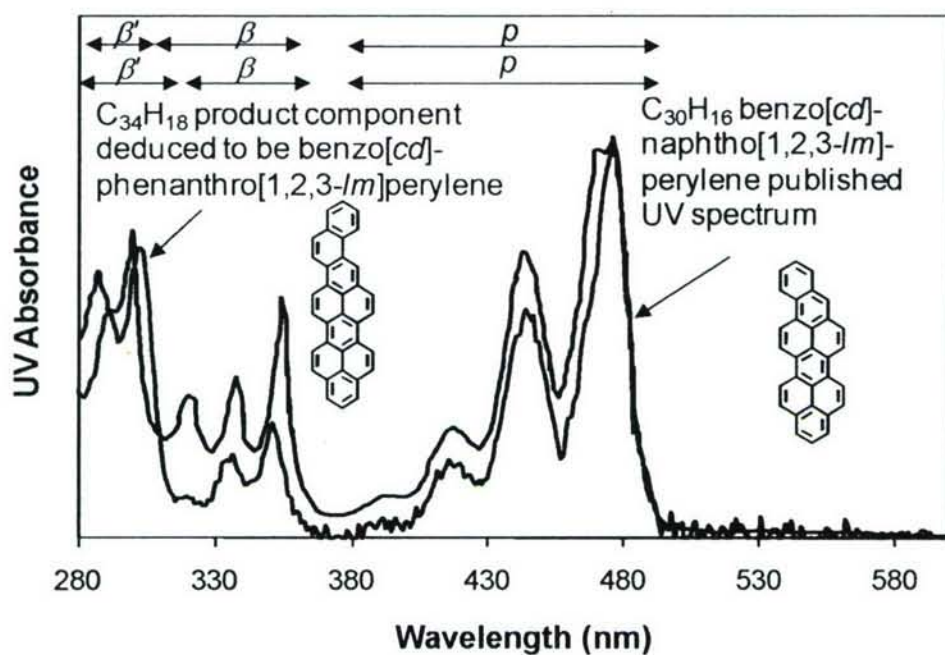


Figure 18. UV spectrum (in red) of the 1-methylnaphthalene product component eluting at 174 min in Figure 17, along with the published [25,51] UV spectrum (in black) of benzo[*cd*]naphtho[1,2,3-*lm*]perylene. Results from Somers and Wornat [42].

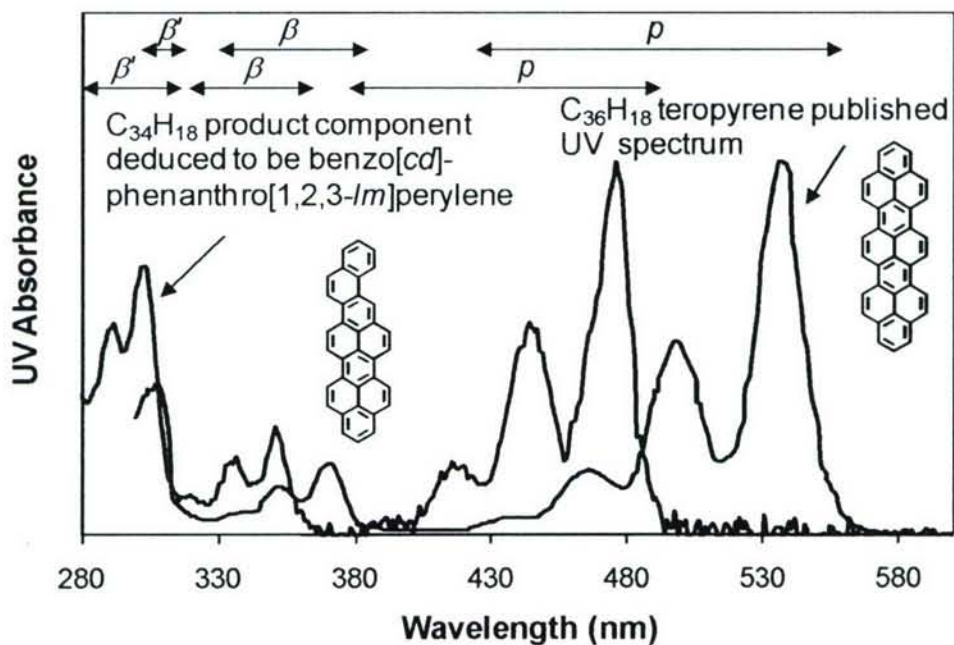


Figure 19. UV spectrum (in red) of the 1-methylnaphthalene product component eluting at 174 min in Figure 17, along with the published [57] UV spectrum (in black) of teropyrene. Results from Somers and Wornat [42].

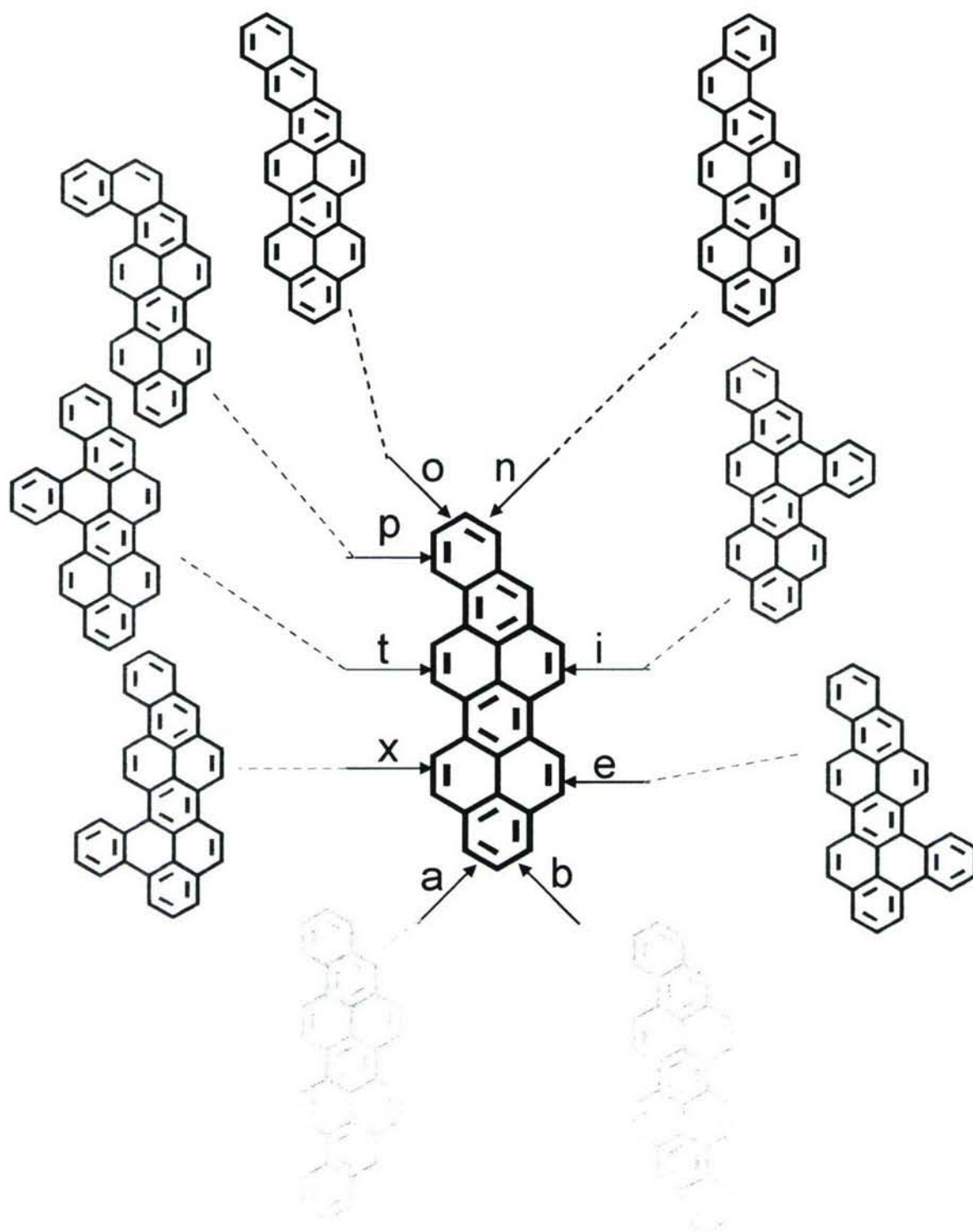


Figure 20. Benzo[cd]naphtho[1,2,3-*lm*]perylene and the 9 possible benzenoid C₃₄H₁₈ that can result from ring fusion to benzo[cd]naphtho[1,2,3-*lm*]perylene. Benzo[cd]phenanthro[1,2,3-*lm*]perylene, shown in red, is deduced [42] to be the 1-methylnaphthalene product component eluting at 174 min in Figure 17.

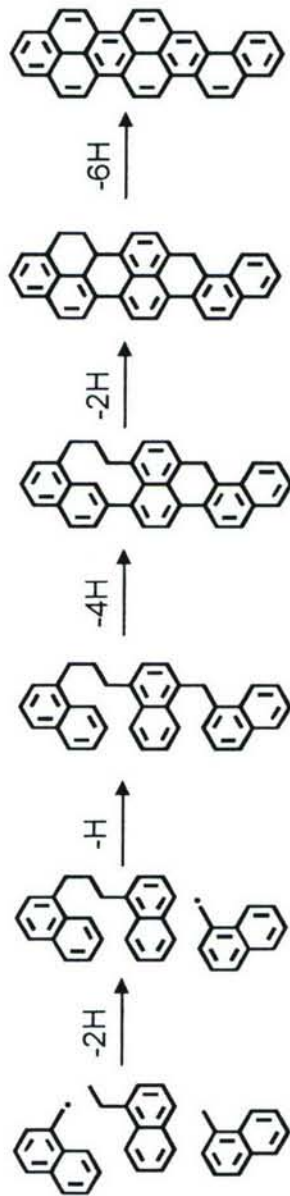


Figure 21. Proposed reaction mechanism [42] for benzo[cd]phenanthro[1,2,3-*m*]perylene.

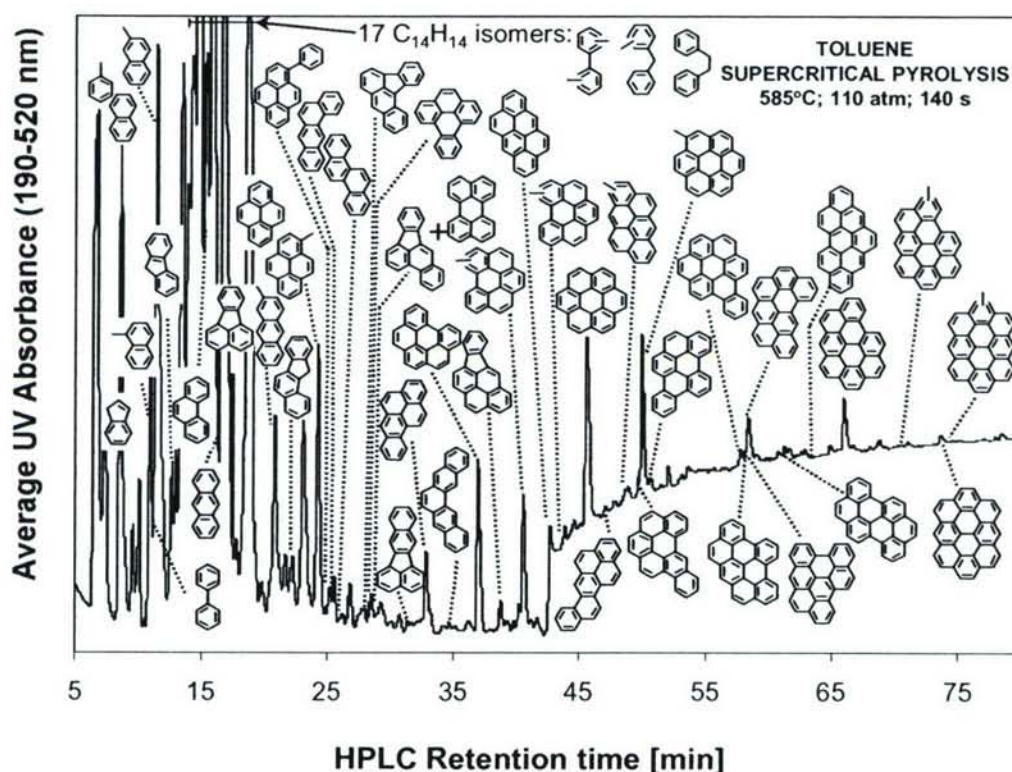


Figure 22. HPLC chromatogram of products of supercritical toluene pyrolysis at 535°C, 100 atm, and 140 s residence time. The rise in the baseline at ~43 min is due to a change in the mobile phase to the UV-absorbing dichloromethane. Identified components, in order of elution, from left to right, are: toluene, indene, naphthalene, 1-methylnaphthalene, bi-phenyl, 2-methylnaphthalene, fluorene, phenanthrene, anthracene, fluoranthene, pyrene, 2-methylanthracene, benzo[*a*]fluorene, 1-methylpyrene, 1-phenylpyrene, benz[*a*]anthracene, chrysene, benzo[*a*]fluoranthene, benzo[*e*]pyrene, benzo[*b*]fluoranthene co-eluting with perylene, benzo[*k*]fluoranthene, benzo[*a*]pyrene, pentaphene, benzo[*ghi*]perylene, indeno[1,2,3-*cd*]pyrene, methylated benzo[*ghi*]perylene, anthanthrene, methylated benzo[*ghi*]perylene, coronene, naphtho[2,1-*a*]pyrene, methylated anthanthrene, dibenzo[*b,ghi*]perylene, 1-methylcoronene, dibenzo[*e,ghi*]perylene, benzo[*a*]coronene, phenanthro[5,4,3,2-*efghi*]perylene, benzo[*cd*]naphtho[8,1,2,3-*fghi*]perylene, benzo[*ghi*]naphtho[8,1,2-*bcd*]perylene, benzo[*pqr*]naphtho[8,1,2-*bcd*]perylene, tribenzo[*cd,ghi,lm*]perylene, naphtho[8,1,2-*abc*]coronene, methylated naphtho[8,1,2-*abc*]coronene, ovalene, and methylated ovalene. Red structures correspond to C₂₈H₁₄ PAH. Data from McClaine and Wornat [17].

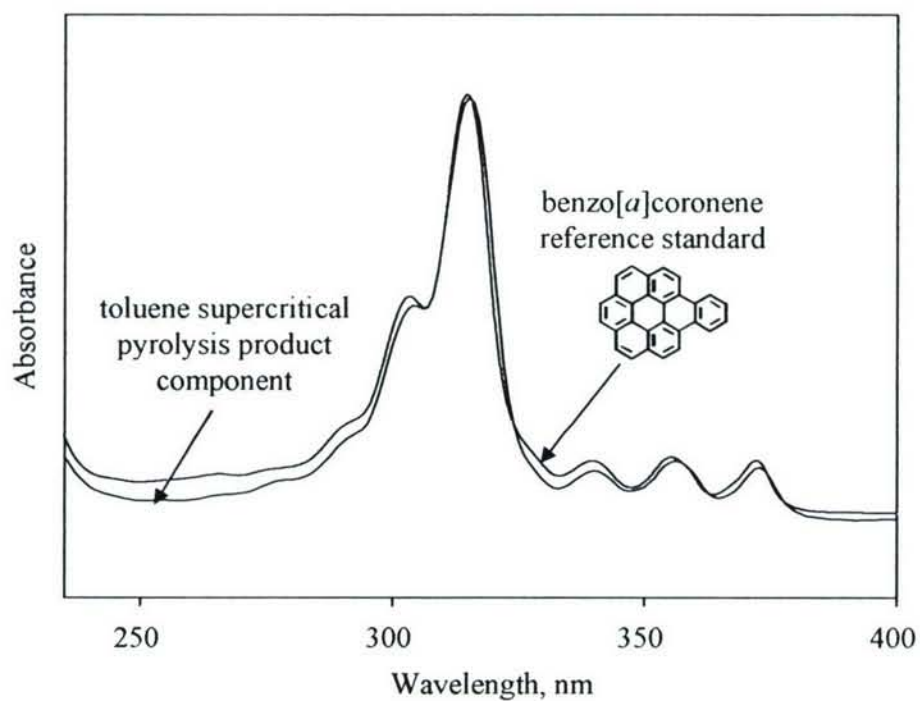


Figure 23. UV absorbance spectra of the reference standard of benzo[a]coronene (red) and of a supercritical toluene pyrolysis product component (black). Results from Wornat *et al.* [61].

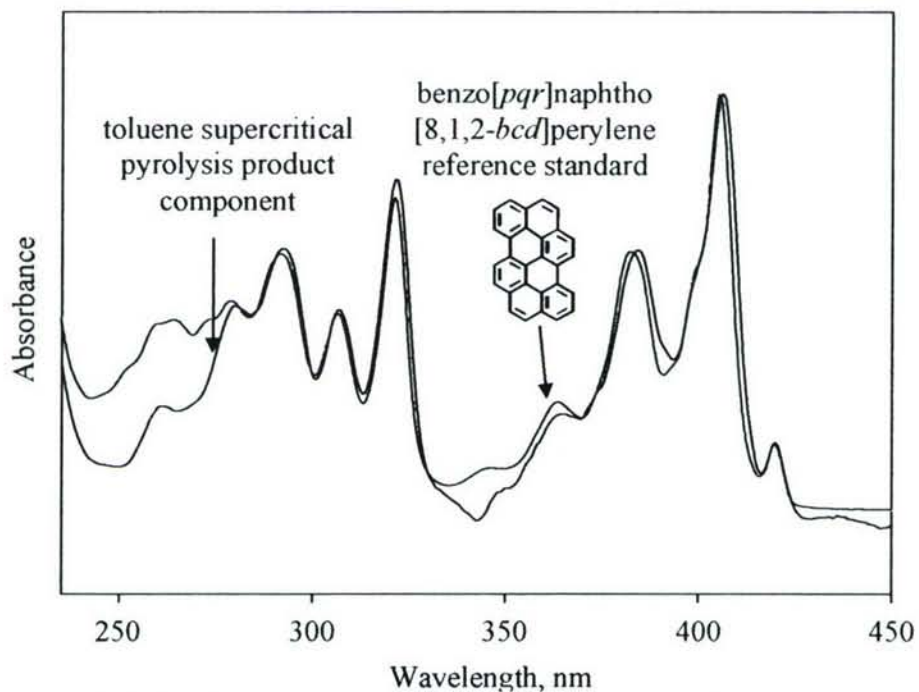


Figure 24. UV absorbance spectra of the reference standard of benzo[pqr]naphtho[8,1,2-bcd]perylene (red) and of a supercritical toluene pyrolysis product component (black). Results from Wornat *et al.* [61].

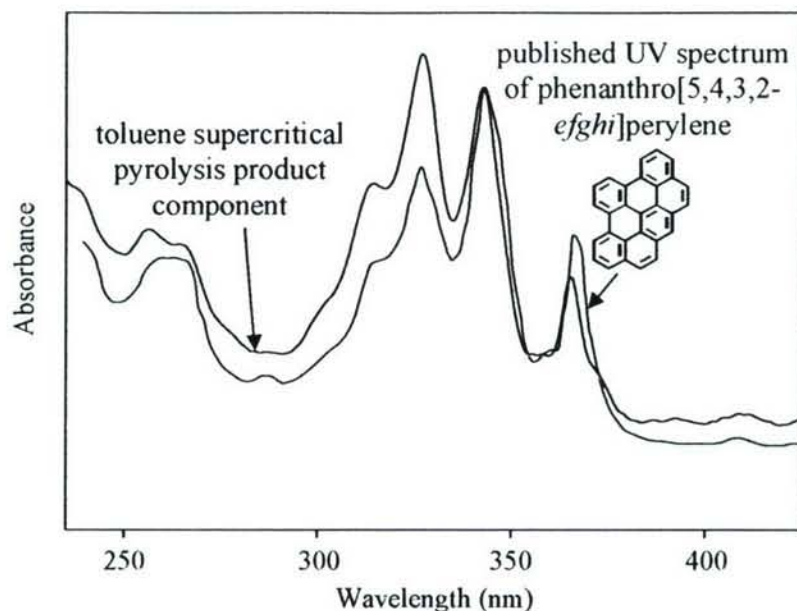


Figure 25. UV absorbance spectra of the reference standard [65] of phenanthro[5,4,3,2-*efghi*]perylene and of a supercritical toluene pyrolysis product component. The spectral peak at 315 nm is interference from the UV spectrum of benzo[*a*]coronene, which elutes just before phenanthro[5,4,3,2-*efghi*]perylene in Figure 22. Results from Wornat *et al.* [61].

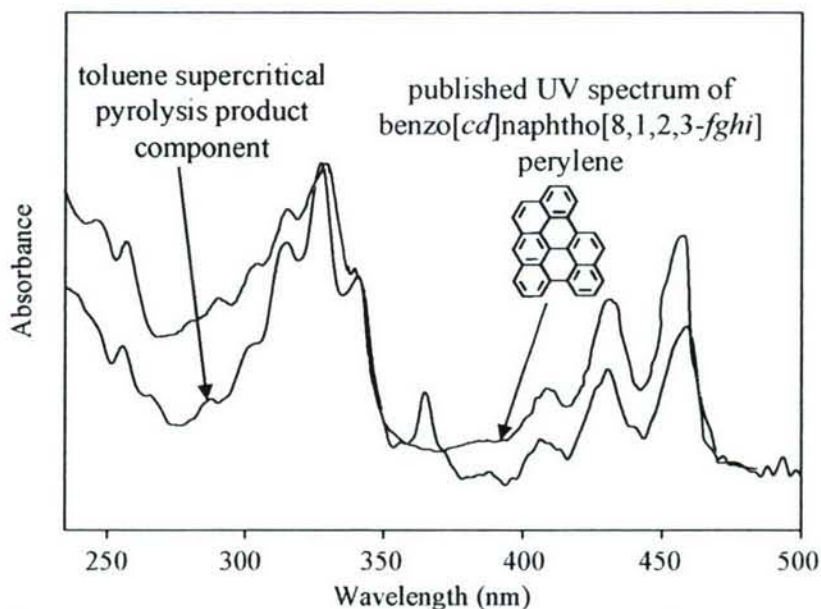


Figure 26. UV absorbance spectra of the reference standard [66,67] of benzo[*cd*]naphtho[8,1,2,3-*fghi*]perylene, in ethanol, and of a supercritical toluene pyrolysis product component, in dichloromethane and acetonitrile. The spectrum of the reference standard has been shifted 2.5 nm to the right to correct for differences in the solvents' indices of refraction [73,74]. The spectral peak at 366 nm is interference from the UV spectrum of phenanthro[5,4,3,2-*efghi*]perylene, which elutes just before benzo[*cd*]naphtho[8,1,2,3-*fghi*]perylene in Figure 22. Results from Wornat *et al.* [61].

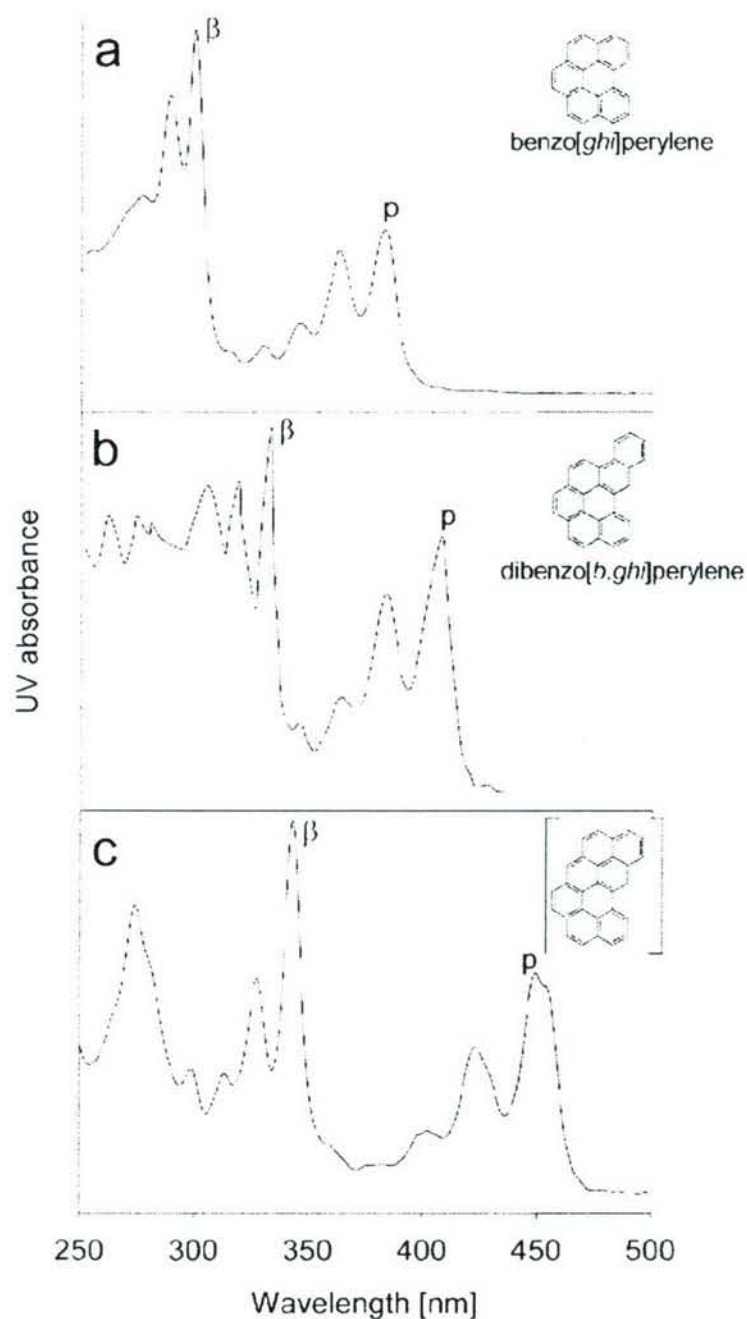


Figure 27. UV spectra for (a) benzo[*ghi*]perylene in acetonitrile, (b) dibenzo[*b,ghi*]perylene [69] in ethanol (before 280 nm) and benzene (after 280 nm), and (c) the C₂₈H₁₄ supercritical toluene products component deduced [58] to be benzo[*ghi*]naphtho[8,1,2-*bcd*]perylene, in 25:75 acetonitrile:dichloromethane. The structures of the PAH are shown to the right of the UV spectra. The structures in (a) and (b) are from the respective reference standards; the bracketed structure shown in (c) is that deduced [58] for the toluene product component.

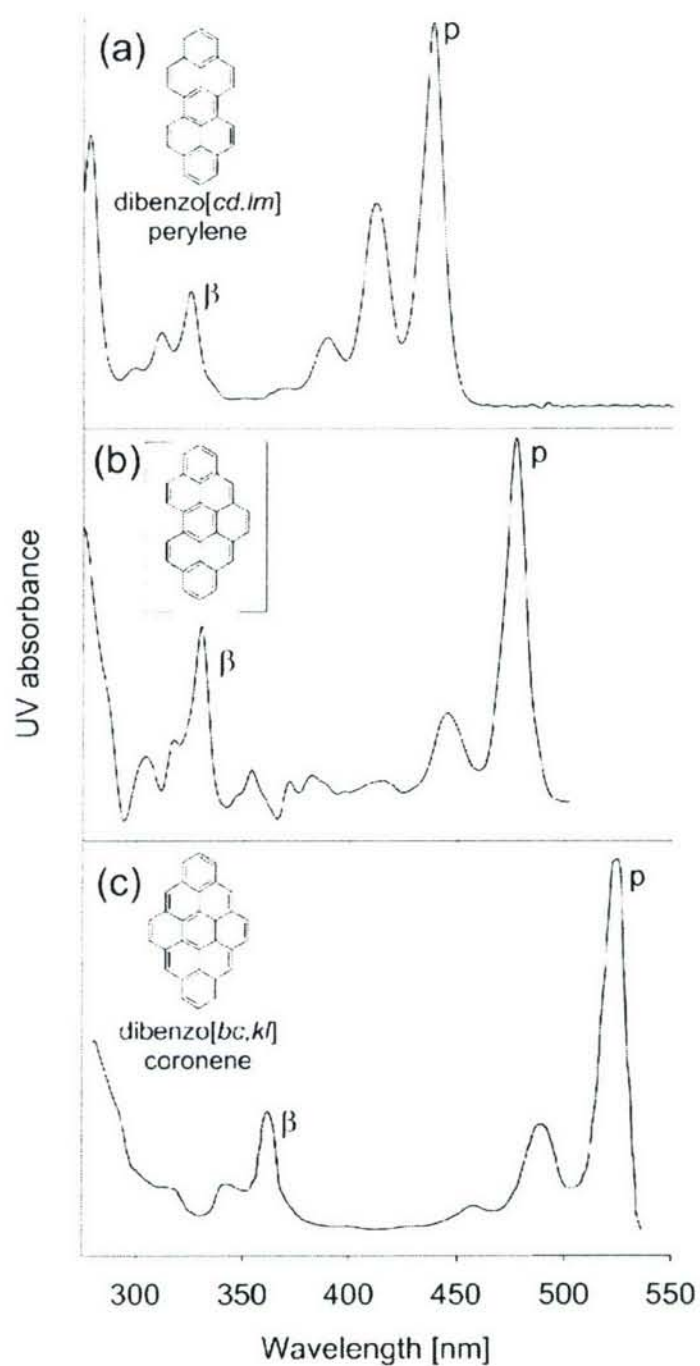


Figure 28. UV spectra for (a) dibenzo[cd,lm]perylene in benzene, (b) the $C_{28}H_{14}$ supercritical toluene products component deduced [68] to be tribenzo[cd,ghi,lm]perylene, in 25:75 methanol:dichloromethane, and (c) dibenzo[bc,kl]coronene [49] in 1-methylnaphthalene. The structures of the PAH are shown to the left of the UV spectra. The structures in (a) and (c) are from the respective reference standards; the bracketed structure shown in (b) is that deduced [68] for the toluene product component.

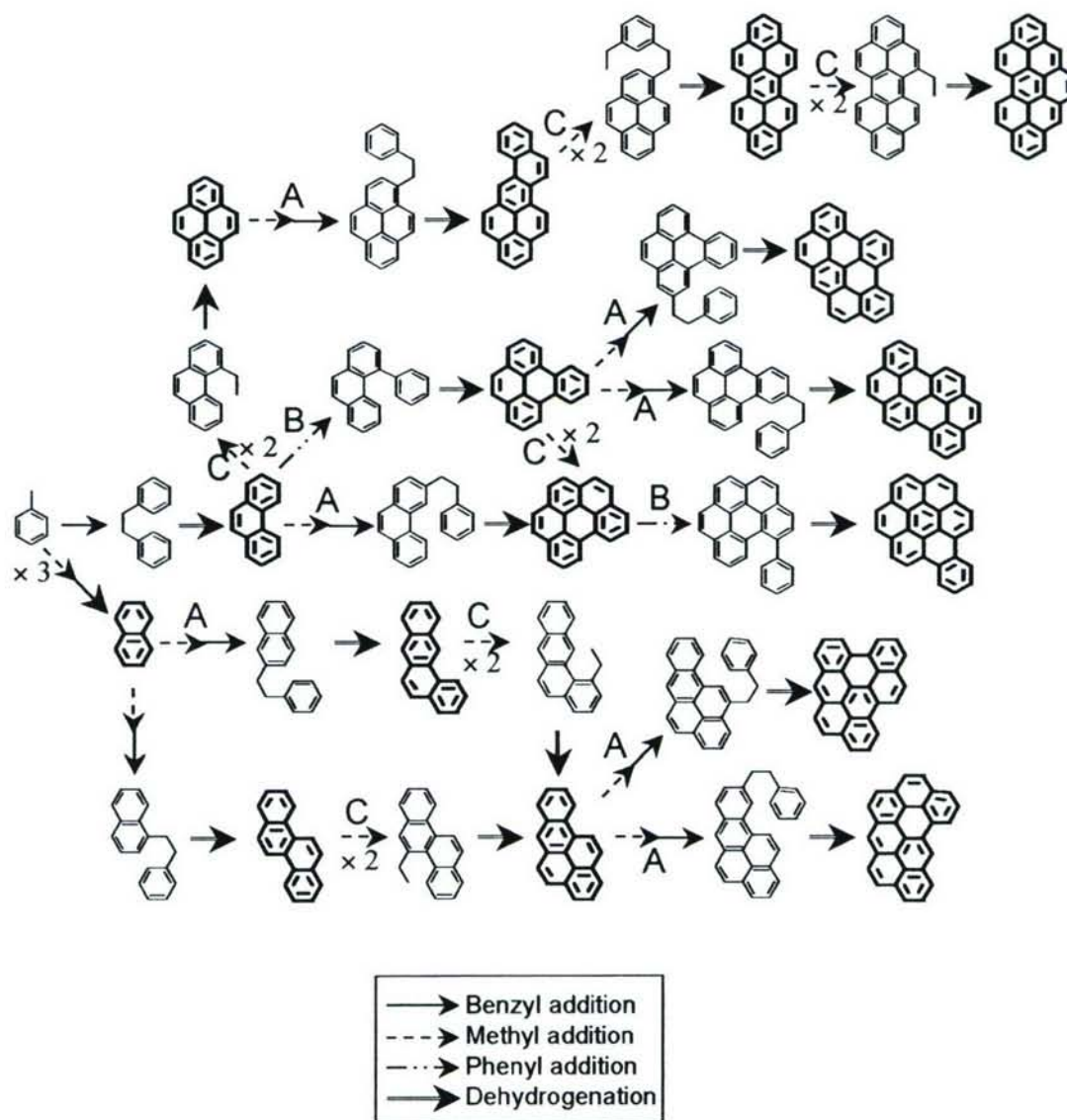


Figure 29. Reaction mechanisms to describe the formation of the six $C_{28}H_{14}$ PAH (shown in red) produced by supercritical toluene pyrolysis. In order from top to bottom, the $C_{28}H_{14}$ PAH are: tribenzo[*cd,ghi,lm*]perylene, phenanthro[5,4,3,2-*efghi*]perylene, benzo[*pqr*]naphtho[8,1,2-*bcd*]perylene, benzo[*a*]coronene, benzo[*cd*]naphtho[8,1,2,3-*fghi*]perylene, and benzo[*ghi*]naphtho[8,1,2-*bcd*]perylene. The formation of large PAH is shown through addition of methyl (dashed arrow), benzyl (solid arrow), and phenyl (dashed-dotted arrow) radicals. Dehydrogenation is shown as the double-lined arrow. In general, the three types of reactions are: (A) addition of methyl followed by benzyl, (B) addition of phenyl, and (C) addition of two methyls. Structures in bold print are PAH that have been identified, by their UV spectra, as products of the supercritical pyrolysis of toluene. Results from McClaine and Wornat [17].

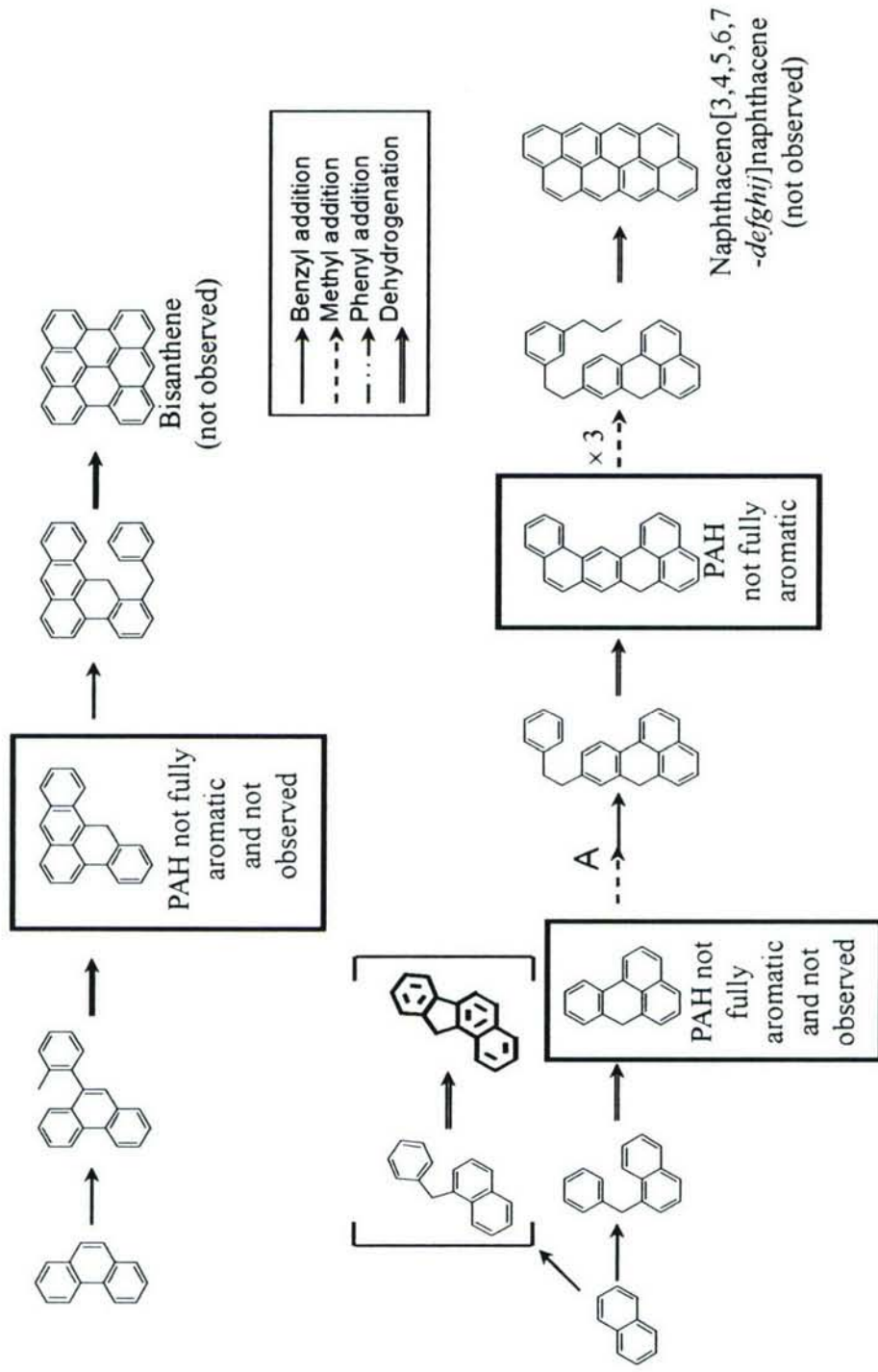


Figure 30. Attempted formation of the two benzenoid $C_{28}H_{14}$ PAH found not to be produced by supercritical toluene pyrolysis: bisanthrene and naphthaceno[3,4,5,6,7-defghi]naphthacene. "A" signifies addition of methyl followed by benzyl, as indicated in Figure 29. Results from McClaine and Wornat [17].

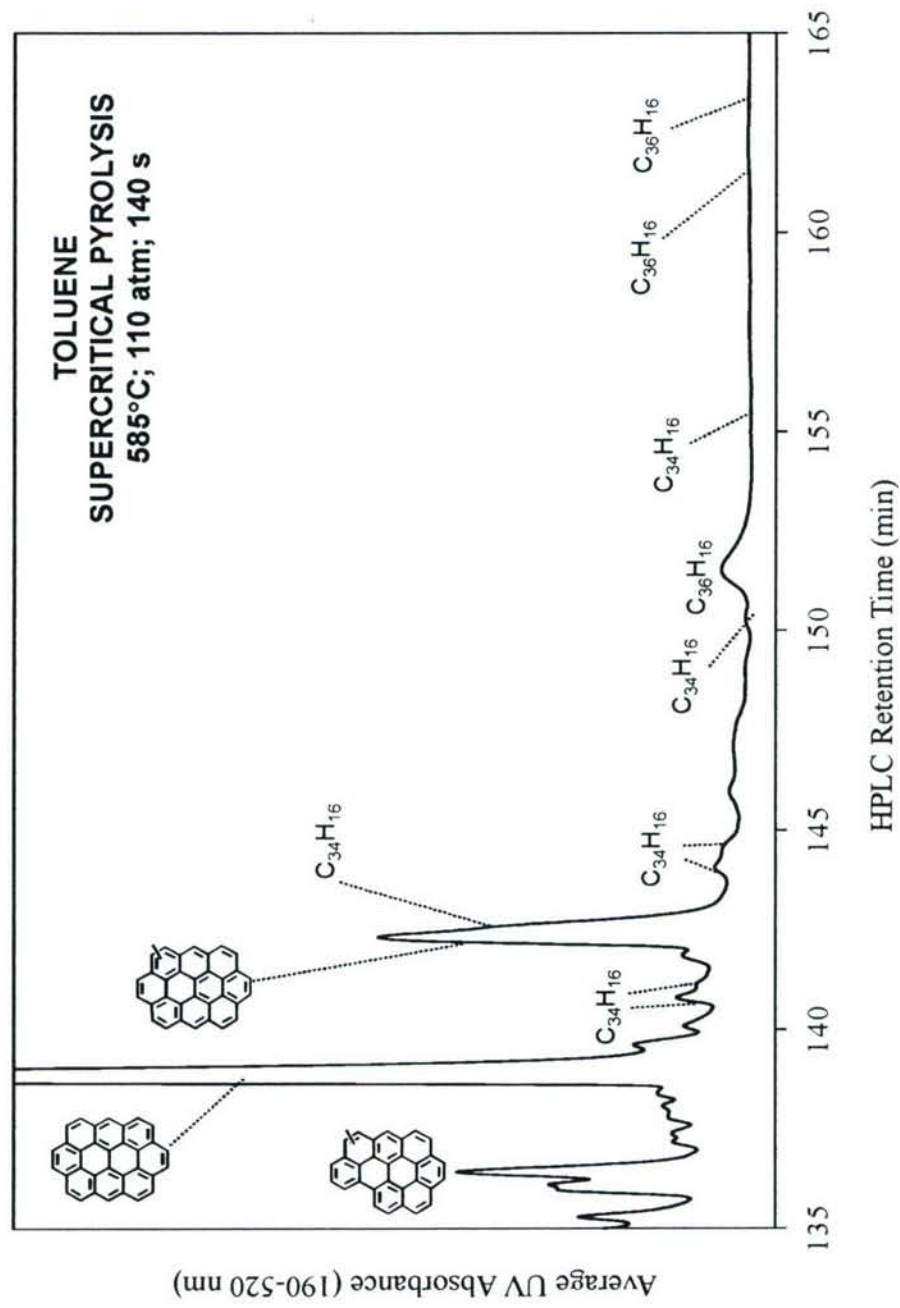


Figure 31. Final portion of the HPLC chromatogram (from the methanol/dichloromethane alternative solvent program) of the products of toluene pyrolyzed at 585°C, 110 atm, and 140 sec. Peaks labeled $C_{34}H_{16}$ and $C_{36}H_{16}$ correspond to 10- and 11-ring PAH products, respectively.

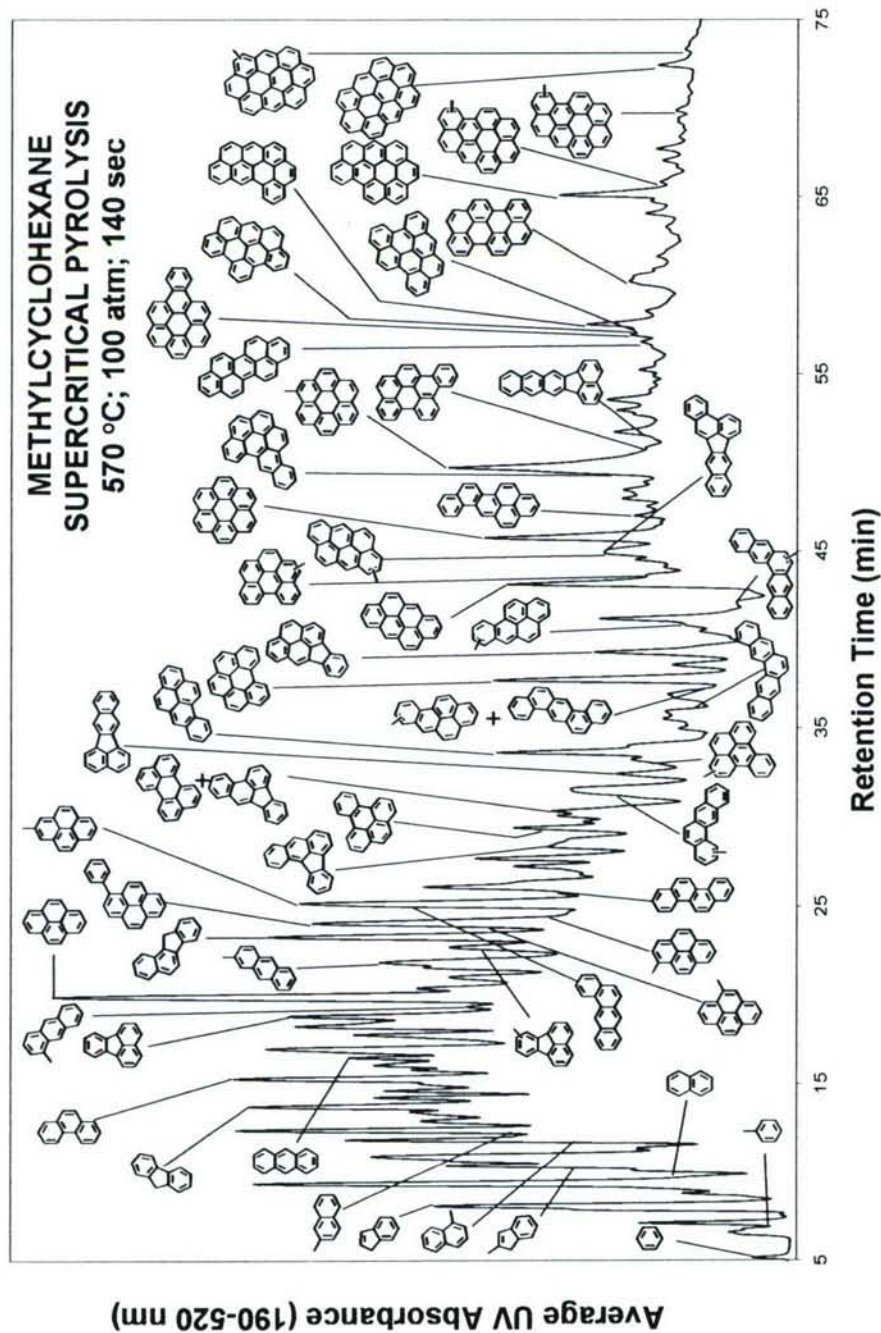


Figure 32. HPLC chromatogram of products of methylcyclohexane pyrolyzed at 570 °C, 100 atm and 140 sec. The rise in baseline at ~43 min corresponds to a change in mobile-phase composition to UV-absorbing dichloromethane. Identified components, in order of elution from left to right, are: benzene, toluene, indene, naphthalene, 2-methylindene, 1-methylnaphthalene, 2-methylnaphthalene, fluorene, phenanthrene, anthracene, fluoranthene, 1-methylantracene, pyrene, 2-methylantracene, alkylfluoranthene, benzo[a]fluorene, 4-methylpyrene, 1-phenylpyrene, 1-methylpyrene, benz[a]anthracene 2-methylpyrene, chrysene, benzo[a]fluoranthene, benzo[e]pyrene, benzo[b]fluoranthene co-eluting with perylene, alkylbenzo[a]anthracene, benzo[k]fluoranthene, alkylbenzo[e]pyrene, benzo[a]pyrene, pentaphene, alkylbenzo[a]pyrene co-eluting with dibenz[a,h]anthracene, benzo[ghi]perylene, indeno[1,2,3-cd]pyrene, alkylbenzo[a]pyrene, alkylpentaphene, anthanthrene, alkylbenzo[ghi]perylene, alkylanthanthrene, dibenzo[b,k]fluoranthene, coronene, naphtho[2,1-a]pyrene, dibenzo[b,ghi]perylene, 1-methylcoronene, dibenzo[e,ghi]perylene, naphtho[2,3-k]fluoranthene, dibenzo[cd,lm]perylene, benzo[a]coronene, phenanthro[5,4,3,2-e]perylene, benzo[cd]naphtho[8,1,2,3-ghi]perylene, benzo[ghi]naphtho[8,1,2-bcd]perylene, benzo[pqr]naphtho[8,1,2-bcd]perylene, naphtho[8,1,2-abc]coronene, alkylnaphtho[8,1,2-abc]coronene, ovalene, and alkylvalene.

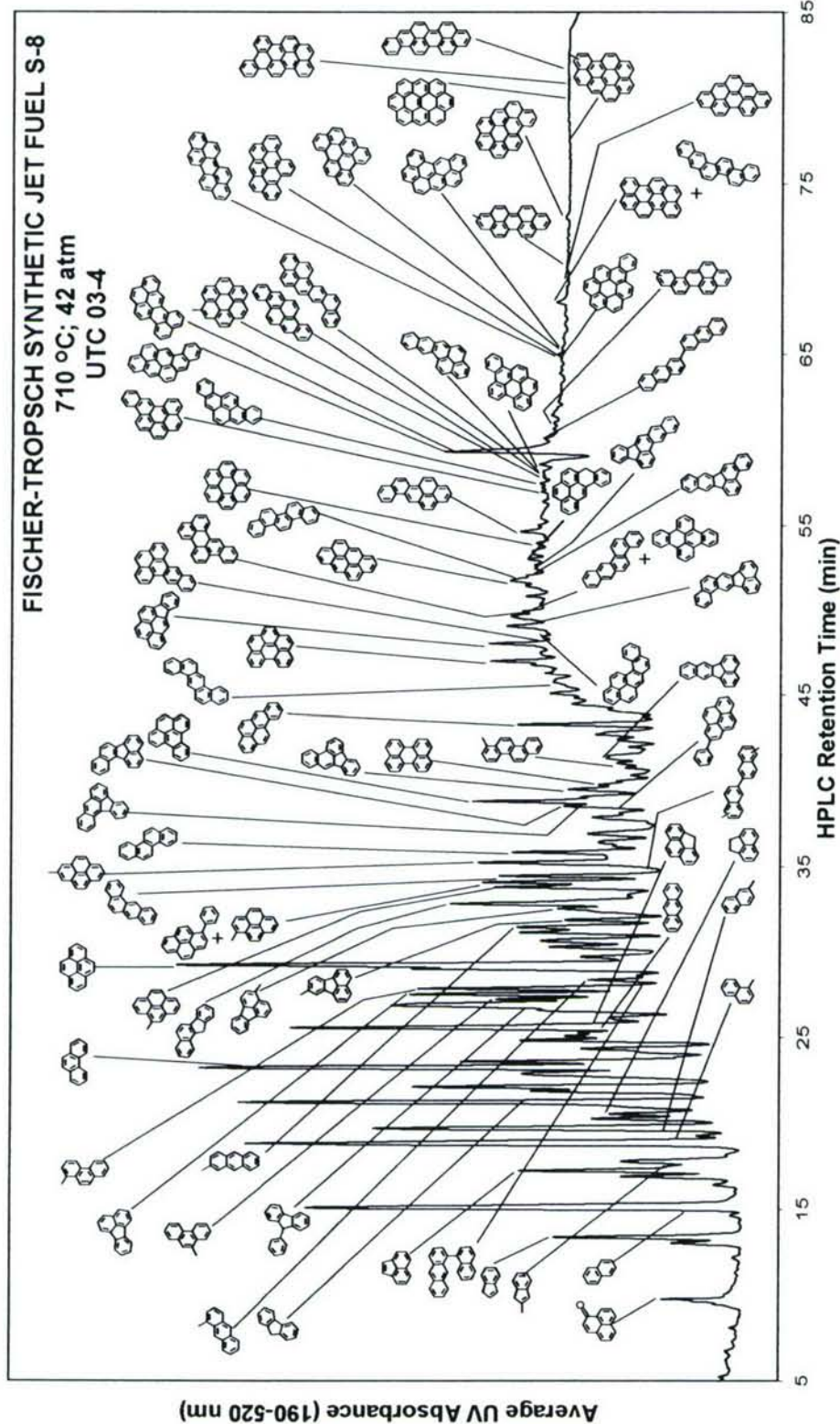


Figure 33. HPLC chromatogram of products of Fischer-Tropsch synthetic jet fuel S-8, pyrolyzed at 710 °C and 42 atm, in a scramjet test rig at UTRC. The rise in baseline at ~43 min corresponds to a change in mobile-phase composition to UV-absorbing dichloromethane. Identified components, in order of elution from left to right, are: phenalenone, indene, naphthalene, acenaphthylene, 2-methylindene, 1-methylnaphthalene, 2-methylnaphthalene, acenaphthene, phenanthrene, anthracene, cyclopenta[def]phenanthrene, 9-phenylfluorene, 9-methylphenanthrene, fluoranthene, 1-methylphenanthrene, 1,1'-naphthylanthracene, 1-methylanthracene, pyrene, 2-methylanthracene, 8-methylfluoranthene, 3-methylfluoranthene, benzo[a]fluoranthene, 4-methylpyrene, 1-phenylpyrene, benz[a]anthracene, 2,2'-binaphthyl, 2-methylpyrene, chrysene, 2-phenylpyrene, benzo[j]fluoranthene, benzo[a]fluoranthene, benzo[e]pyrene, benzo[b]fluoranthene, perylene, 1-methylchrysene, benzo[k]fluoranthene, benzo[a]pyrene, dibenz[a,h]anthracene, benzo[ghi]perylene, indeno[1,2,3-cd]pyrene, naphtho[2,3-e]pyrene, naphtho[1,2-a]pyrene, naphtho[1,2-k]fluoranthene, benzo[b]perylene, benzo[b]chrysene coeluting with dibenzo[e]pyrene, anthanthrene, picene, dibenzo[b,k]fluoranthene, naphtho[2,3-b]fluoranthene, 8H-dibenz[a,k]pyrene, coronene, naphtho[2,1-a]pyrene, dibenzo[b,ghi]perylene, dibenzo[a,l]pyrene, 1-methylcoronene, phenanthro[2,3-a]pyrene, naphtho[2,3-a]pyrene, dibenzo[e,ghi]perylene, benzo[a]anthracene, naphtho[8,1,2-bcd]perylene, dibenzo[a,h]pyrene, 2,2'-bianthryl, alkylnaphtho[2,1-a]pyrene, dibenzo[cd,lm]perylene, benzo[a]coronene, phenanthro[5,4,3,2-efgh]perylene, benzo[cd]naphtho[8,1,2,3-fghi]perylene, benzo[ghi]naphtho[8,1,2-bcd]perylene, benzo[cd,lm]perylene co-eluting with benzo[b]picene, tribenzo[cd,ghi,lm]perylene, alkyldibenzo[cd,lm]perylene, naphtho[8,1,2-abc]coronene, alkylnaphtho[8,1,2-bcd]perylene, dibenzo[e,ghi]naphtho[8,1,2-k]perylene and benzo[cd]naphtho[1,2,3-m]perylene.

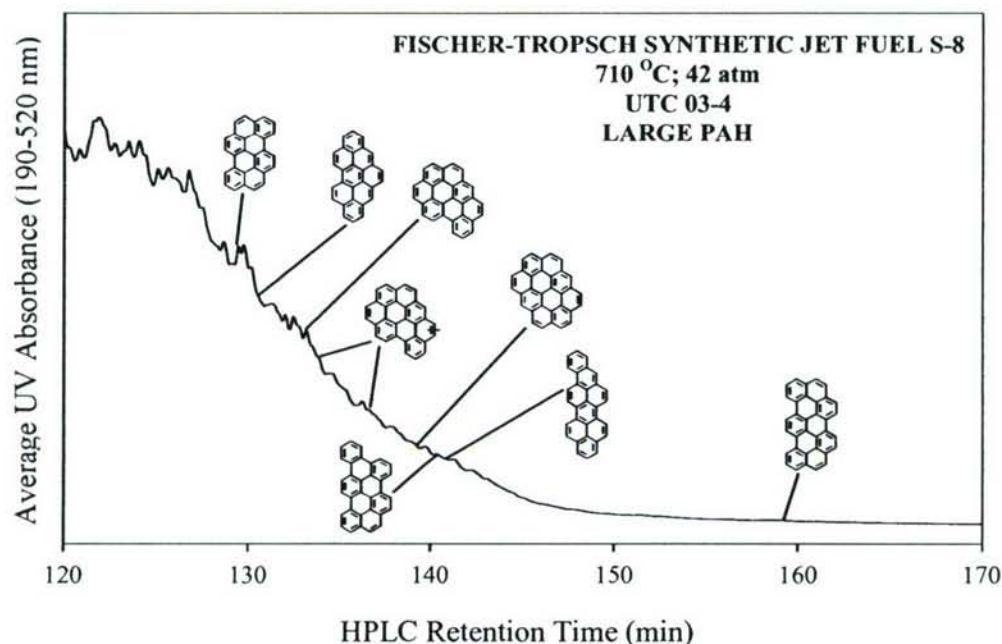


Figure 34. Final portion of the HPLC chromatogram (from a methanol/dichloromethane solvent program) of the products of Fischer-Tropsch synthetic jet fuel S-8, pyrolyzed at 710 °C and 42 atm, in a scramjet test rig at UTRC.

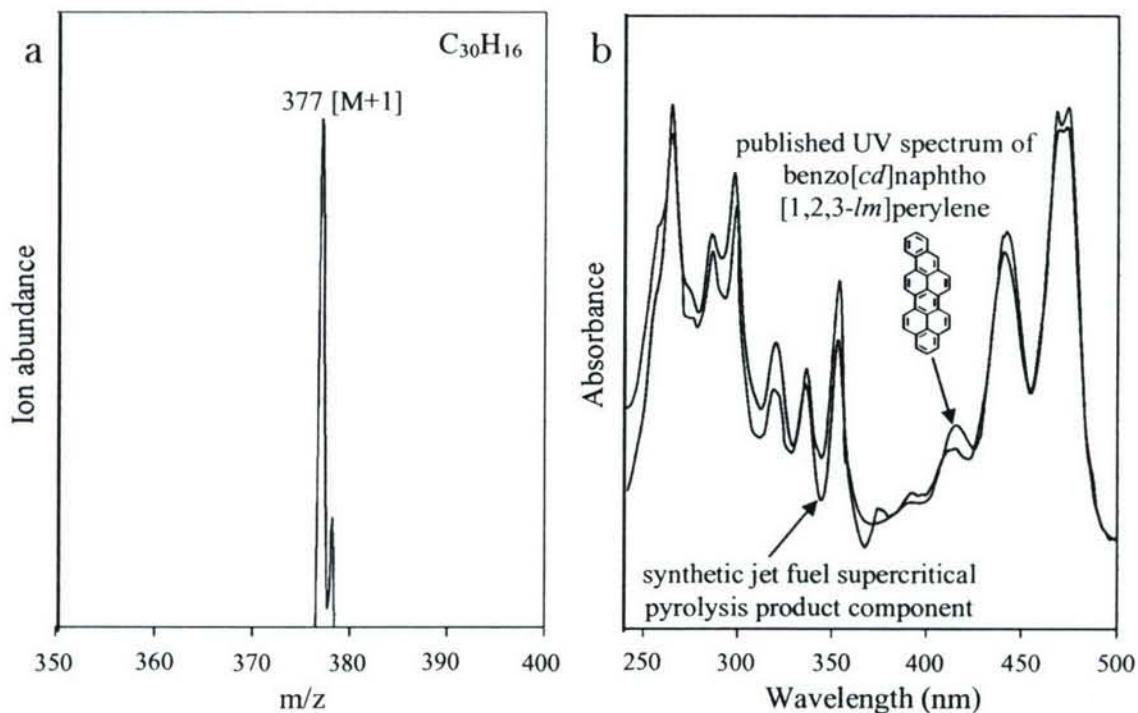


Figure 35. The (a) mass spectrum and (b) UV spectrum of the supercritical Fischer-Tropsch synthetic jet fuel S-8 pyrolysis product component eluting at 141 min in Figure 34. Due to proton transfer from the solvent dichloromethane, the primary ion in the mass spectrum is at $M+1$, so $M = 376$. The published [25,51] UV spectrum of a reference standard of benzo[cd]naphtho[1,2,3-*lm*]perylene is included in (b) to confirm the product component's identity as benzo[cd]naphtho[1,2,3-*lm*]perylene.